J. Fluid Mech. (1979), *vol.* 92, *part* 1, *pp.* 171–205
Printed in Great Britain

Laminar flow of an incompressible fluid past a bluff body: the separation, reattachment, eddy properties and drag

By F. T. SMITH

Department of Mathematics, Imperial College, London

(Received 6 March 1978)

The asymptotic theory for the laminar, incompressible, separating and reattaching flow past the bluff body is based on an extension of Kirchhoff's (1869) free-streamline solution. The flow field (only the upper half of which is discussed since we consider a symmetric body and flow) consists of two basic parts. The first is the flow on the body scale l^*, which is described to leading order by the Kirchhoff solution with smooth inviscid separation, but with an $O(Re^{-\frac{1}{16}})$ modification to explain fully the viscous separation (here Re ($\gg 1$) is the Reynolds number). The influence of this $Re^{-\frac{1}{16}}$ modification is determined for the circular cylinder. The second part is the large-scale flow, comprising mainly the eddy and the ultimate wake. The eddy has length scale $O(Re\, l^*)$, width $O(Re^{\frac{1}{2}} l^*)$ and is of elliptical shape to keep the eddy pressure almost uniform. The ultimate wake is determined numerically and fixes the eddy length. The (asymptotically small) back pressure from the eddy acts (on the body scale) both in the free stream and in the eddy, and it has a marked effect at moderate Reynolds numbers; combined with the Kirchhoff solution, it predicts the pressure drag on a circular cylinder accurately, to within 10 % when $Re = 5$ and to within 4 % when $Re = 50$. Other predictions, for the eddy length and width, the front pressure and the eddy pressure, also show encouraging agreement with experiments and Navier–Stokes solutions at moderate Reynolds numbers (of about 30), both for the circular cylinder and the normal flat plate. Finally, an analysis in the appendix indicates that, in wind-tunnel experiments, the tunnel walls (even if widely spaced) can exert considerable influence on the eddy properties, eventually forcing an upper bound on the eddy width as Re increases instead of the $O(l^* Re^{\frac{1}{2}})$ growth appropriate to the unbounded flow situation.

1. Introduction

Over the years there have been many attempts at providing a theoretical description, for high Reynolds numbers, of the two-dimensional laminar streaming motion of an incompressible fluid past a bluff body. For convenience, we shall confine our discussion here to the symmetric flow problem, in which the body possesses an axis of symmetry which is aligned with the uniform stream at infinity, so that only the upper half of the flow field need be considered. Most of the attempts referred to above have recognized the fact that the inviscid attached flow solution bears no relation to the behaviour of a real fluid because of the contradiction that the associated boundary layer on the body almost inevitably approaches a spurious, and singular (Goldstein 1948), separation ahead of the rear stagnation point; the only real exception to such a contradiction could occur if the body were very streamlined towards its rear and had a

0022-1120/79/4205-6290 $02.00

trailing edge of vanishingly small angle (Roshko 1967; Professor K. Stewartson 1977, private communication). Accordingly, efforts have been concentrated on trying to deal with the separation phenomenon and/or with the eddy of circulatory flow between separation and reattachment. Prior to a discussion (given below) of the separation involved, it is convenient to consider the eddy models, many of which have aimed at a turbulent flow description rather than the laminar flow theory which is our concern, and which we categorize into three broad types (*a*), (*b*) and (*c*), as follows.

Type (*a*) is an extension of the Kirchhoff (1869) free-streamline model, in which it is assumed that the eddy behind the body consists of nearly stagnant fluid at the same pressure as that of the undisturbed stream. This model is often called, somewhat misleadingly, 'an infinite (or open) wake model'; but a more appropriate term is 'a large eddy model'. For, in the extended Kirchhoff model, the eddy length and height, rather than being infinite, simply have the property that they are both much greater than the typical body dimension (l^*, say), a property which is in fact not contrary to experimental and numerical experience (see below). The model has been considered by Squire (1934), Imai (1953), Kawaguti (1953) and, more fully, by Professor A. F. Messiter (private communications), Messiter (1975) and Sychev (1967).

Type (*b*) is the free-streamline model, in which the eddy is again nearly stagnant but is not at the free-stream pressure. As a consequence the eddy is either of finite dimensions, $O(l^*)$, or contains some anomalous features (as in the Riabouchinsky (1919) or Gilbarg & Serrin (1950) proposals). Investigations of this model have been made by Woods (1955), Roshko (1954, 1955), Wu (1956, 1962), Lighthill (1949) and Southwell & Vaisey (1946).

Type (*c*) contains all the models in which the typical eddy velocity is comparable with the undisturbed stream velocity U_∞^*, implying usually that the pressure at the eddy surface is not uniform. These models include the Prandtl–Batchelor eddy of constant vorticity (Batchelor 1956), the Föppl (1913) vortex model (see also Shair 1963), the variable-pressure work of Woods (1955), the proposal by Grove *et al.* (1964) and Acrivos *et al.* (1965, 1968) of an eddy of finite width but great length (see however the appendix below), and the wake source models of Parkinson & Jandali (1970) and Kiya & Arie (1977) (see also Wu 1968, 1972; Birkhoff & Zarantonello 1957).

None of the models of type (*b*) or (*c*) has proved entirely successful from the viewpoint of a rational, laminar flow, theory. Indeed the serious objections to types (*b*) and/or (*c*) are manifold. First, experience from reliable experimental and numerical (Navier–Stokes) investigations (Grove *et al.* 1964; Dennis & Chang 1970) has shown that the eddy length grows, virtually linearly, with increasing Reynolds number Re, contrary to the postulates of models with finite eddies. Second, the velocities within the eddy do tend to be relatively small in practice. Third, the analytical problems posed by those models which assume (implicitly or otherwise) eddy velocities of the order of U_∞^* are probably overspecified and insoluble. For the analyst is then left with the awesome task of ensuring that the eddy flow produces closed streamlines, that the eddy pressure balances that of the exterior flow at the dividing streamline, that the behaviour of the eddy near the inviscid breakaway point is consistent with viscous separation (see below), and that the drag on the body is only small. No flow solution satisfying all these requirements has ever been found. Fourth, there must be consistency between the inviscid description of breakaway of the dividing streamline from the body and the viscous account of separation. In models with finite eddy

velocities this consistency requirement implies that the eddy flow itself must induce a secondary separation, at some distance from the main separation of the dividing streamline. While such secondary separation cannot be discounted, there is certainly no firm evidence in favour of its occurrence (in steady flow, at least). In fact, all the relevant numerical and experimental evidence so far tends to support the view that only the single, main, separation occurs; that the approaching upstream boundary layer on the body is completely lifted away from the surface by this separation and then forms a viscous shear layer, and that, near the body at least, the eddy flow, being relatively slow, is simply entrained into the viscous shear layer surrounding the dividing streamline and is then swept downstream. Finally, a fifth objection is raised by Acrivos *et al.* (1965) concerning the pressure recovery in the wake.

One may now be even more specific about the fourth point of the previous paragraph, concerning the need for reconciliation between the inviscid breakaway and the viscous separation. For a first (and, we suggest, the only) self-consistent account of the incompressible viscous separation involved here has only recently been found [F. T. Smith 1977, following Sychev's (1972) proposal; see also Messiter & Enlow 1973; Messiter 1975]. This account is based on triple-deck theory (Stewartson 1974) and it explains how the attached boundary layer on the body upstream of the inviscid breakaway point separates abruptly in the neighbourhood of the breakaway point and then emerges from the separation zone as a free shear layer surrounding the dividing streamline. The account demands that, to leading order, the inviscid breakaway must be of the *smooth* type, i.e. the dividing streamline must have only finite curvature at the breakaway point. The account also demands that the perturbation to the inviscid flow field is $O(Re^{-\frac{1}{16}})$ and that near the breakaway point the perturbation must exhibit a particular singularity, the exact form of which is specified by the triple-deck viscous separation [see F. T. Smith 1977; and (2.3a, b) below].

The above self-consistent description of the separation and breakaway might be fitted into any of the eddy models (a), (b) and (c) in principle. But, given all the previously mentioned serious objections to the overall models of types (b) and (c), we attempt to provide in this paper a theoretical account of the entire high Reynolds number laminar motion past the bluff body based on the extended Kirchhoff model (a) and on the triple-deck separation. It is found that a complete multi-structured description can indeed be made, both for the flow at finite distances from the body (the 'body-scale flow' of §2) and for the larger-scale motion comprising the eddy and the eventual wake (§3). Comparisons of most features of the theoretical body-scale flow with experiments and Navier–Stokes solutions at moderate Reynolds numbers strongly support the present approach (see §2.4, figures 3–5 and §§4 and 5 for the drag), while other features are, at the least, readily reconcilable with the observed and calculated behaviour. Comparisons (in §3.3) of the larger-scale flow are even more encouraging (see figures 8–10), especially for the eddy length, which is predicted in §3.2, and the near-eddy pressure, predicted in §3.1. In particular, the theory here enables us to resolve the often-quoted discrepancies between observation and the Kirchhoff model *per se* as regards the drag on the body and the eddy pressure. For the lower-order effects greatly improve the theoretical predictions of both quantities, bringing the differences between theory and experiments or calculations to within about 10% at Reynolds numbers of the order of 30. The most important of these lower-order effects is the (asymptotically small) back pressure due to the eddy; in

§4 it is shown that this back pressure simply imposes a rescaling on the body-scale flow properties. The reason for the rescaling is that the back pressure is exerted *uniformly* at large distances from the body rather than just within the eddy, a feature which is in contrast with the anomalous effects of back pressure in previous studies [see the eddy models of type (*b*) above]. Also, an analysis given in the appendix indicates that experimental measurements of eddy properties (e.g. eddy width or pressure) are significantly affected by the presence of confining walls even when the walls are widely spaced and that, therefore, theories (e.g. Acrivos *et al.* 1965, 1968) based on those experiments are inappropriate to the unbounded flow problem. The only doubt (see §3.1) about the overall model adopted here concerns the flow properties near reattachment, where we propose a passive behaviour, similar to that of Burggraf (1975), Jenson, Burggraf & Rizzetta (1974), Smith & Duck (1977) and Professor K. Stewartson (1977, private communication), instead of the backward-jet behaviour of Messiter, Hough & Feo (1973). A discussion is given in §5.

The motion is assumed to be laminar, steady and two-dimensional throughout. Also, the kind of bluff body we have principally in mind is one which is smooth except possibly for a trailing edge of finite angle, although the large-scale theory of §3 applies also to non-smooth bluff bodies, an extreme example of which is the broadside-on flat plate considered in §3.3. The Reynolds number Re is defined by

$$Re = U_\infty^* l^*/\nu^* \quad (\gg 1), \tag{1.1}$$

where ν^* is the kinematic viscosity of the incompressible fluid, and we shall work with the non-dimensional velocities u and v in the x and y directions and the non-dimensional pressure p. Here x, y, u, v and p have been non-dimensionalized with respect to l^*, l^*, U_∞^*, U_∞^* and $\rho^* U_\infty^{*2}$, in turn, where ρ^* is the fluid density and x denotes the direction of the undisturbed stream $u = 1$. The stream function is ψ, where

$$u = \partial\psi/\partial y,$$

$v = -\partial\psi/\partial x$ and $\psi = 0$ on the body. The undisturbed stream is taken to be at zero pressure.

2. The body-scale flow

The 'body-scale flow' describes the motion at distances $O(1)$ or less from the body. We let q be the flow speed $(u^2+v^2)^{\frac{1}{2}}$. The body-scale flow then has ψ, u, q and p generally $O(1)$ [$(\psi, u, q, p) = (\psi_1, u_1, q_1, p_1) + o(1)$, say], except in the viscous layers or reversed flow zones referred to below.

We consider the various regions of the body-scale flow in §§2.1–2.3 below, showing that a complete self-consistent account seems possible. Then §2.4 compares the body-scale flow obtained from the present asymptotic theory with Navier–Stokes solutions and experiments at moderate Reynolds numbers.

2.1. *The main flow regions* (I, III, V)

The Kirchhoff (1869) free-streamline model adopted here assumes that the free streamline $\psi = 0 = \hat{n}$ breaks away from the body at an unknown position $\hat{\theta} = \hat{\theta}_{\text{sep}} > 0$, where $\hat{\theta}$ and $\hat{n}$ signify respectively distances along and normal to the body surface and

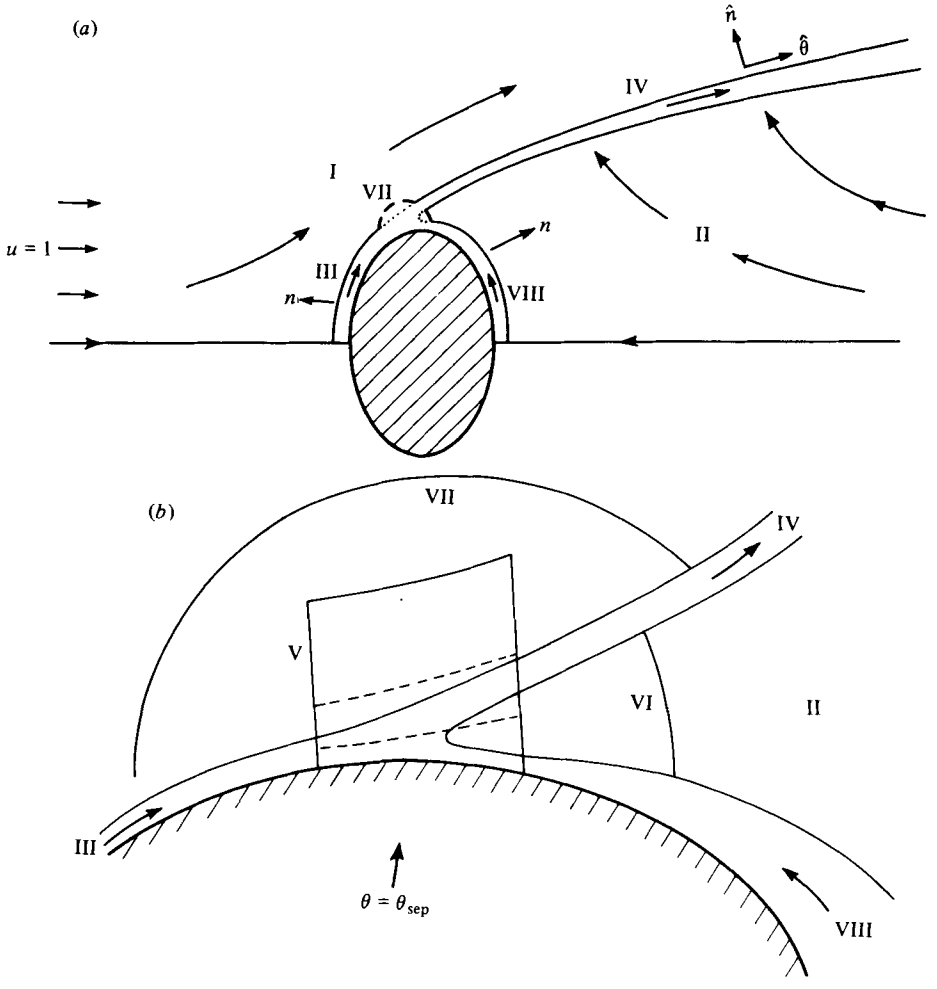

FIGURE 1. (*a*) The overall structure of the body-scale flow, and co-ordinates. (*b*) The flow structure near separation.

free streamline $\psi = 0$, with $\hat{\theta} = 0$ at the front stagnation point. The model postulates further that $q_1 = 1$ and $p_1 = 0$ on the free streamline downstream of the breakaway (see figure 1). Behind the breakaway, in the near-eddy region II between the free streamline [described by $y = D_1(x) + o(1)$] and the line of symmetry ($y = 0$),

$$\psi_1 = u_1 = q_1 = p_1 = 0,$$

so that only a relatively slow flow is expected there (see §2.3 below). The solution of $\nabla^2\psi_1 = 0$ for the inviscid potential flow in region I, outside the near-eddy II and the viscous layers III and IV (figure 1), is then fixed by the condition of *smooth separation* imposed on the pressure along $\hat{n} = 0$:

$$\left.\begin{aligned} p_1 &\sim k_1(\hat{\theta}_{sep} - \hat{\theta})^{\frac{3}{2}} \quad \text{as} \quad \hat{\theta} \to \hat{\theta}_{sep}, \\ p_1 &= 0 \quad \text{for} \quad \hat{\theta} > \hat{\theta}_{sep}. \end{aligned}\right\} \tag{2.1a}$$

Here k_1 is a (positive) constant not known in advance. The required behaviour (2.1*a*)

serves to fix both the dividing-streamline shape $y = D_1(x)$ and the value of $\hat{\theta}_{\rm sep}$, in particular (while if (2.1a) is not imposed, p_1 has a square-root singularity at breakaway and the breakaway is inconsistent with viscous separation; F. T. Smith 1977, p. 446). From (2.1a), if the distance of the free streamline $\psi = 0$ from the surface is

$$S(\hat{\theta}) = S_1(\hat{\theta}) + o(1),$$

we have

$$\left.\begin{aligned} &S_1 \sim (\hat{\theta}-\hat{\theta}_{\rm sep})^2/2a + \tfrac{2}{5}k_1(\hat{\theta}-\hat{\theta}_{\rm sep})^{\frac{5}{2}} \quad \text{as} \quad \hat{\theta}\rightarrow\hat{\theta}_{\rm sep}^{+}, \\ &S_1 = 0 \quad \text{for} \quad \hat{\theta} < \hat{\theta}_{\rm sep}, \end{aligned}\right\} \tag{2.1b}$$

where a is the radius of curvature of the body at $\hat{\theta} = \hat{\theta}_{\rm sep}$. In general, the pressure gradient $\partial p_1/\partial\hat{\theta}$ at the surface is favourable throughout $0 \leqslant \hat{\theta} < \hat{\theta}_{\rm sep}$, so the $O(Re^{-\frac{1}{2}})$ boundary layer III (figure 1) stays attached for $\hat{\theta} < \hat{\theta}_{\rm sep}$, its scaled skin friction $\partial u(\hat{\theta}, 0)/\partial N$ (where $\hat{n} = Re^{-\frac{1}{2}}N$ in III) tending to a positive $O(1)$ value λ as $\hat{\theta}\rightarrow\hat{\theta}_{\rm sep}^{-}$. The viscous separation near $\hat{\theta} = \hat{\theta}_{\rm sep}$ then occurs abruptly, within a triple-deck structure V. It is provoked by an $O(Re^{-\frac{1}{16}})$ perturbation in the main flow field I:

$$(\psi, u, q, p) = (\psi_1, u_1, q_1, p_1) + Re^{-\frac{1}{16}}(\psi_2, u_2, q_2, p_2) + \ldots, \tag{2.2}$$

where $\nabla^2\psi_2 = 0$ and the combined flow field (2.2) satisfies the Kirchhoff conditions on the body and free streamline. The perturbation in (2.2) remains small throughout I (and, indeed, forces a relative error $O(Re^{-\frac{1}{16}})$ through the entire flow field); but the triple-deck structure V governing the abrupt separation near $\hat{\theta} = \hat{\theta}_{\rm sep}$ demands the local behaviour, along $\hat{n} = 0$,

$$\left.\begin{aligned} &p_2 \sim -\alpha\lambda^{\frac{2}{3}}(\hat{\theta}_{\rm sep}-\hat{\theta})^{\frac{1}{2}} \quad \text{as} \quad \hat{\theta}\rightarrow\hat{\theta}_{\rm sep}^{-}, \\ &p_2 = 0 \quad \text{for} \quad \hat{\theta} > \hat{\theta}_{\rm sep}, \end{aligned}\right\} \tag{2.3a}$$

where $\alpha \doteqdot 0{\cdot}44$ (Smith 1977). Hence the $O(Re^{-\frac{1}{16}})$ perturbation dominates the inviscid behaviour close to separation. The increasingly adverse pressure gradient which it promotes as $\hat{\theta}\rightarrow\hat{\theta}_{\rm sep}^{-}$ is exactly consistent with the requirements of triple-deck viscous separation (F. T. Smith 1977), and the triple-deck account explains how the singularity in the inviscid behaviour (2.3a) is smoothed out [over a distance $O(Re^{-\frac{3}{8}})$] as the fluid passes through separation. We move on, therefore, to the remaining features of the body-scale flow.

2.2. *The flow just outside the triple-deck separation* (*regions* V, VI)

At distances just greater than $O(Re^{-\frac{3}{8}})$ beyond the separation, the entire viscous layer III emerges from the triple deck as a free shear layer IV of thickness $O(Re^{-\frac{1}{2}})$ centred around the dividing streamline

$$S \sim \tfrac{2}{3}\alpha\lambda^{\frac{2}{3}}Re^{-\frac{1}{16}}(\hat{\theta}-\hat{\theta}_{\rm sep})^{\frac{3}{2}}, \tag{2.3b}$$

the form (2.3b) following from (2.3a). The velocity at the upper edge of the free shear layer is effectively the free-stream velocity, while at the lower edge the velocity is effectively zero. The shear layer therefore entrains fluid, at a rate given by

$$\psi|_{\hat{n}\rightarrow 0-} \sim -C_0\lambda^{\frac{1}{3}}Re^{-\frac{1}{2}}(\hat{\theta}-\hat{\theta}_{\rm sep})^{\frac{3}{2}} \tag{2.4}$$

for $0 < \hat{\theta}-\hat{\theta}_{\rm sep} \ll 1$, where $C_0 = 1{\cdot}2521\ldots$.

Apart from the triple deck, the local adjustment near separation is then completed by two inviscid zones: VI, lying beneath the shear layer, between the triple deck and

the near eddy II; and VII, lying above the shear layer, between the triple deck and the main flow field I. The first zone encountered (VI) is necessary to achieve *inter alia* a gradual modification of the dividing-streamline shape, from the form (2.3*b*) emerging from the triple deck to the form (2.1*b*) holding at the start of the main flow field I. From (2.1*b*) and (2.3*b*), VI is set up when $(\hat{\theta}-\hat{\theta}_{\rm sep})$ is $O(Re^{-\frac{1}{8}})$. Therefore let

$$\theta = \theta_{\rm sep} + Re^{-\frac{1}{8}}\theta_A$$

in VI, where θ and n denote distances along and normal to the body surface respectively (so that $\theta = \hat{\theta}$ and $n = \hat{n}$ for $\hat{\theta} < \hat{\theta}_{\rm sep}$). Then, in VI, $n = Re^{-\frac{1}{8}}n_A$ from (2.1*b*) and (2.3*b*), and to leading order

$$(\psi, q, p) = (Re^{-\frac{7}{8}}\psi_A, \quad Re^{-\frac{1}{8}}q_A, \quad \pi_E + Re^{-\frac{2}{8}}p_A), \tag{2.5}$$

where π_E is an undetermined $o(1)$ pressure constant (see (3.2*b*) below). The orders of magnitude in (2.5) stem from the behaviour

$$p \propto -Re^{-\frac{1}{4}}[Re^{\frac{3}{8}}(\theta-\theta_{\rm sep})]^{-\frac{5}{3}}, \tag{2.6a}$$

$$q \propto -Re^{-\frac{1}{8}}[Re^{\frac{3}{8}}(\theta-\theta_{\rm sep})]^{-\frac{4}{3}}, \tag{2.6b}$$

$$\psi \propto -Re^{-\frac{3}{4}}[Re^{\frac{3}{8}}(\theta-\theta_{\rm sep})]^{\frac{2}{3}} \tag{2.6c}$$

of the flow solution below the shear layer immediately downstream of the triple deck (see F. T. Smith 1977, pp. 449–450). The controlling equations in VI are the inviscid boundary-layer equations

$$q_A = \frac{\partial\psi_A}{\partial n_A}, \quad q_A\frac{\partial q_A}{\partial\theta_A} - \frac{\partial\psi_A}{\partial\theta_A}\frac{\partial q_A}{\partial n_A} = -\frac{\partial p_A}{\partial\theta_A}, \quad \frac{\partial p_A}{\partial n_A} = 0, \tag{2.7a}$$

where $0 < \theta_A < \infty$ and $0 < n_A < S_A(\theta_A)$. Here $n_A = S_A(\theta_A)$ defines the shape of the dividing streamline through zone VI. The anticipated boundary conditions for (2.7*a*) are

$$\psi_A = 0 \quad \text{at} \quad n_A = 0, \tag{2.7b}$$

$$\psi_A = -C_0\theta_A^{\frac{2}{3}}\lambda^{\frac{1}{3}} \quad \text{at} \quad n_A = S_A(\theta_A)^-, \tag{2.7c}$$

$$\left.\begin{aligned} &\psi_A \sim -C_0\theta_A^{-\frac{5}{6}}\lambda^{\frac{1}{3}}n_A/S_A(\theta_A) && (2.7d)\\ &p_A \sim -(9C_0^2/8\alpha^2)\lambda^{\frac{1}{3}}\theta_A^{-\frac{5}{3}} && (2.7e)\\ &S_A \sim \tfrac{2}{3}\alpha\lambda^{\frac{2}{3}}\theta_A^{\frac{2}{3}} && (2.7f) \end{aligned}\right\} \quad \text{as} \quad \theta_A \to 0+,$$

$$S_A \sim (2a)^{-1}\theta_A^2 \quad \text{as} \quad \theta_A \to \infty. \tag{2.7g}$$

Here (2.7*b*, *c*) ensure tangential flow at the body surface and the entrainment condition (2.4) at the dividing streamline, while (2.7*d*, *e*) match zone VI to the triple deck V at $\theta_A = 0+$ [from (2.6)]. Finally, (2.7*f*, *g*) join the dividing streamline to its upstream shape (2.3*b*) and to its downstream shape (2.1*b*). The required solution of (2.7*a*–*g*) is

$$\psi_A = -C_0\lambda^{\frac{1}{3}}n_A/\{\tfrac{2}{3}\alpha\lambda^{\frac{2}{3}}\theta_A^{\frac{5}{6}} + \theta_A^{\frac{4}{3}}/2a\}, \tag{2.8a}$$

$$q_A = -C_0\lambda^{\frac{1}{3}}/\{\tfrac{2}{3}\alpha\lambda^{\frac{2}{3}}\theta_A^{\frac{5}{6}} + \theta_A^{\frac{4}{3}}/2a\}, \tag{2.8b}$$

$$p_A = -\tfrac{1}{2}q_A^2, \tag{2.8c}$$

$$S_A = \tfrac{2}{3}\alpha\lambda^{\frac{2}{3}}\theta_A^{\frac{2}{3}} + (2a)^{-1}\theta_A^2. \tag{2.8d}$$

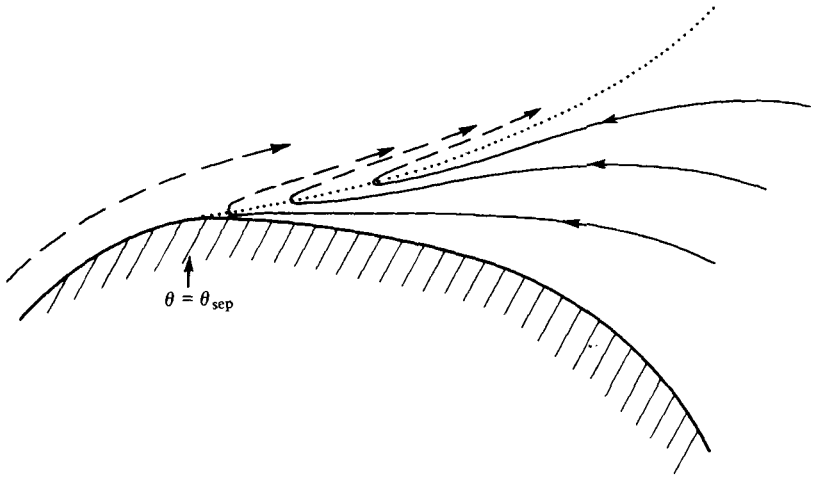

FIGURE 2. The streamlines (solid lines) in the adjustment zone VI just beyond separation.

The adjustment from (2.3b) to (2.1b) is therefore achieved through zone VI and the flow in VI is entirely reversed. The motion in zone VI is sketched in figure 2. Moreover we note for later use that, first, (2.8) implies that as the near-eddy flow II is approached [$S_A \to O(Re^{\frac{1}{8}})$ formally] the velocity and pressure variation become $O(Re^{-\frac{1}{4}})$ and $O(Re^{-1})$ respectively. Second, the backward-facing viscous sublayer between zone VI and the wall is bound to remain attached, since the pressure gradient in (2.8) accelerates the sublayer towards the triple deck; this sublayer then continues into a sublayer of the triple deck (F. T. Smith 1977, p. 450).

The other main adjustment zone VII, outside the shear layer, occurs when $\hat{n}$ and $\hat{\theta} - \hat{\theta}_{sep}$ are both $O(Re^{-\frac{1}{16}})$ and is of a character similar to that of VI. Its purpose is to adjust the potential flow from the triple-deck form [dominated by (2.3a) when

$$Re^{-\frac{3}{8}} \ll |\hat{\theta} - \hat{\theta}_{sep}| \ll Re^{-\frac{1}{16}}]$$

to the dominant Kirchhoff form (2.1a) which holds for $Re^{-\frac{1}{16}} \ll |\theta - \theta_{sep}| \ll 1$. The governing properties in VII are all linear, however, and in particular the pressure adjusts linearly, from (2.3a) to (2.1a), through zone VII, as does the free-streamline shape, from (2.3b) to (2.1b).

2.3. *The shear layer and the near eddy (regions* IV, II, VIII)

The free streamline $\psi = 0$, $y = D_1(x)$, determined by the leading-order potential flow problem in I, develops the well-known property of a parabolic growth downstream:

$$D_1(X) \sim bx^{\frac{1}{2}} \quad \text{as} \quad x \to \infty. \tag{2.9}$$

The constant b here is related to the leading-order drag $C_{D\infty}$ on the whole body, in the form

$$b = (4C_{D\infty}/\pi)^{\frac{1}{2}} \tag{2.10}$$

necessary for global conservation of momentum in the potential flow. Also, in general $b > 0$ since the pressure p_1 acting on the body is non-negative and so produces a positive $O(1)$ drag $C_{D\infty}$. Hence, as the eddy length is large (see § 3 below), the eddy

width, given by the continuation of (2.9), must also be large. Again, for $\hat{r} \gg 1$, with $y > S(x)$,

$$\left.\begin{aligned} p_1 &\sim \tfrac{1}{2} b \hat{r}^{-\frac{1}{2}} \sin \tfrac{1}{2}\phi, \\ \psi_1 &\sim y - b\hat{r}^{\frac{1}{2}} \cos \tfrac{1}{2}\phi, \end{aligned}\right\} \tag{2.11}$$

where $\hat{r}$ and ϕ are polar co-ordinates ($x = \hat{r}\cos\phi$, $y = \hat{r}\sin\phi$). So the velocity and pressure throughout the flowfield fall towards their freestream values and a match with the free stream seems possible (see § 3).

As well as the growth downstream of the near-eddy width (2.9), there is also the growth downstream of the shear layer IV surrounding the free streamline to contend with. During the body-scale flow, layer IV, being the continuation beyond $\hat{\theta} = \hat{\theta}_{\text{sep}}$ of the original attached boundary layer III, has thickness $O(Re^{-\frac{1}{2}})$, so that $\hat{n} = Re^{-\frac{1}{2}}N$, say, $\psi = Re^{-\frac{1}{2}}\hat{\psi}$ and $p \ll 1$ in IV. This layer is governed by the boundary-layer equations

$$q\frac{\partial q}{\partial \hat{\theta}} - \frac{\partial \hat{\psi}}{\partial \hat{\theta}}\frac{\partial q}{\partial N} = \frac{\partial^2 q}{\partial N^2} \tag{2.12a}$$

and the boundary conditions

$$q \to 1, 0 \quad \text{as} \quad N \to \pm\infty. \tag{2.12b,c}$$

Here (2.12*b*, *c*) match the shear-layer flow to the flow in the inviscid regions I and II. The starting profile (at $\hat{\theta} = \hat{\theta}^{+}_{\text{sep}}$) for IV is that of the original boundary layer III but with a $(\hat{\theta} - \hat{\theta}_{\text{sep}})^{\frac{1}{2}}$ singularity emanating from the triple deck. Far downstream ($\hat{\theta} \to \infty$) the Chapman form (Lock 1951)

$$\hat{\psi} = \hat{\theta}^{\frac{1}{2}} G(\hat{\eta}) \quad (\hat{\eta} = N/\hat{\theta}^{\frac{1}{2}}), \tag{2.13a}$$

where

$$G''' + \tfrac{1}{2}GG'' = 0, \quad G'(\infty) = 1, \quad G'(-\infty) = 0, \tag{2.13b}$$

is expected. Here $G(\hat{\eta})$ has the property $G(-\infty) = -1{\cdot}24$ ($\equiv -\bar{\kappa}$), in line with the fluid entrainment by the shear layer throughout the range $\hat{\theta}_{\text{sep}} < \hat{\theta} < \infty$ [so that, if $\hat{\psi}(\hat{\theta}, -\infty) = -\hat{\kappa}(\hat{\theta})$, then $d\hat{\kappa}/d\hat{\theta} > 0$ for all $\hat{\theta} > \hat{\theta}_{\text{sep}}$ and $\hat{\kappa}(\hat{\theta}_{\text{sep}}) = 0$].

In the near-eddy II we suggest that the flow is provoked by the above $O(Re^{-\frac{1}{2}})$ entrainment into the shear layer IV. Therefore ψ is $O(Re^{-\frac{1}{2}})$ in II and, since x and y are $O(1)$, u and v are also $O(Re^{-\frac{1}{2}})$ in II. Hence the pressure variation is $O(Re^{-1})$. Notice that these orders for the velocity and pressure variation coincide with the orders implied by § 2.2 [see also (2.16) and (2.17) below]. We write $(\psi, u, q, p) = (Re^{-\frac{1}{2}}\tilde{\psi}, Re^{-\frac{1}{2}}\tilde{u}, Re^{-\frac{1}{2}}\tilde{q}, Re^{-1}\tilde{p} + \pi_E)$ in the near-eddy, the small pressure constant π_E arising from the match with the adjustment zone VI [see (2.8) and (3.2*b*) below]. The motion in the near-eddy is controlled essentially by the inviscid equations $(\tilde{\mathbf{u}}.\nabla)\tilde{\mathbf{u}} = -\nabla\tilde{p}$ and $\operatorname{div}\tilde{\mathbf{u}} = 0$. Therefore

$$\nabla^2\tilde{\psi} = -\tilde{f}(\tilde{\psi}), \tag{2.14a}$$

where the vorticity $\tilde{f}$ is an unknown function of $\tilde{\psi}$. The boundary conditions on $\tilde{\psi}$ are

$$\tilde{\psi} = 0 \quad \text{at} \quad y = 0 \quad \text{and at} \quad n = 0, \tag{2.14b}$$

$$\tilde{\psi} = -\hat{\kappa}(\hat{\theta}) \quad \text{at} \quad y = D_1(x)^{-}, \tag{2.14c}$$

the former being required for symmetry and for tangential flow at the body and the latter to account for the entrainment necessary to maintain the shear layer IV surrounding the free streamline $y = D_1(x)$. To satisfy the entrainment condition in (2.14*c*) there must be a small but non-zero supply of fluid from downstream ($x \to \infty$),

since the near-eddy is not closed on the body scale [$x, y = O(1)$], from (2.9). This necessity leads to the discussion (in § 3 below) of the complete eddy and the reattachment which must ensue far downstream; but here we may infer that the necessary supply is given by a (weak) uniform streaming of the form

$$\tilde{u} \approx -\tilde{c} \quad \text{(constant)}, \quad \tilde{\psi} \approx -\tilde{c}y \quad \text{for} \quad x \gg 1 \quad \text{with} \quad 0 \leqslant y \leqslant bx^{\frac{1}{2}}, \quad (2.14d)$$

where, to conserve mass, $b\tilde{c} = 1{\cdot}24$. The complete solution of (2.14a) is then fixed by the constraints (2.14b, c, d), the last of which implies that

$$\tilde{f} = 0, \tag{2.15}$$

so that the near-eddy is a potential flow region.

Finally, the match between the near-eddy II and the adjustment zone VI near $\hat{\theta} = \hat{\theta}_{\text{sep}}$ may be verified. For, if we use the similarity co-ordinate $\tilde{\eta} = n/(\theta - \hat{\theta}_{\text{sep}})^2$, which is $O(1)$ in the near-eddy II as $\theta \to \hat{\theta}_{\text{sep}}$, then the entrainment condition (2.14c) becomes

$$\tilde{\psi} = -C_0 \lambda^{\frac{1}{3}} (\theta - \hat{\theta}_{\text{sep}})^{\frac{2}{3}} + O(\theta - \hat{\theta}_{\text{sep}})^{\frac{5}{3}} \quad \text{at} \quad \tilde{\eta} = 1/2a + \tfrac{2}{5} k_1 (\theta - \hat{\theta}_{\text{sep}})^{\frac{1}{2}} + O(\theta - \hat{\theta}_{\text{sep}}) \tag{2.16}$$

near $\theta = \hat{\theta}^+_{\text{sep}}$, from (2.4) and (2.1$b$). Also, $\tilde{\psi} = 0$ at $\tilde{\eta} = 0$, from (2.14b). Hence the near-eddy solution is described by

$$\tilde{\psi} = -C_0 \lambda^{\frac{1}{3}} (\theta - \hat{\theta}_{\text{sep}})^{\frac{2}{3}} 2a\tilde{\eta} [1 - \tfrac{4}{5} a k_1 (\theta - \hat{\theta}_{\text{sep}})^{\frac{1}{2}}] + O(\theta - \hat{\theta}_{\text{sep}})^{\frac{5}{3}} \tag{2.17}$$

as $\theta \to \hat{\theta}^+_{\text{sep}}$ with $\tilde{\eta} = O(1)$. Here (2.17) satisfies the governing equation (2.14a) with (2.15) locally, and the leading term in (2.17), of order $(\theta - \hat{\theta}_{\text{sep}})^{\frac{2}{3}}$, matches identically with the leading-order term emerging from zone VI (as $\theta_A \to \infty$), from (2.8a). Hence the slow flow in the near-eddy is consistent with the faster reversed motion closer to the separation point. In general the near-eddy motion is expected to be entirely reversed. As the fluid in the near-eddy approaches the separation point, it speeds up [giving a uniform velocity profile, from (2.17)] in order to conserve the mass flux entrainment in the narrowing gap between the shear layer and the body. The majority of the near-eddy fluid enters the shear layer IV and is swept downstream before the adjustment zone VI is reached; the remaining fluid passes through the adjustment zone VI and then either enters the shear layer or continues (with increasing speed) towards the separation point to maintain the faster reversed motion at the downstream end of the triple-deck flow. This accelerating reversed flow forces the slow reversed boundary layer VIII [lying between the body and the near-eddy and having thickness $O(Re^{-\frac{1}{4}})$] to become increasingly attached and increasingly thin as the separation point is approached, while the final turning of the remaining reversed flow is achieved within the triple deck, of course. [By contrast, if the reversed velocities in the near-eddy were substantial, e.g. $O(1)$ as in a Prandtl–Batchelor eddy, then the near-eddy would have to decelerate as separation was approached and a secondary separation, of the reversed boundary layer VIII, would be inevitable.]

The proposed structure of the body-scale flow is now complete. On the face of it, the above account contains no inconsistencies, and the remaining difficulties concern only the larger-scale flow properties. Before considering the latter (in § 3), we compare in § 2.4 the above body-scale flow theory with observed and calculated flows at moderate Reynolds numbers.

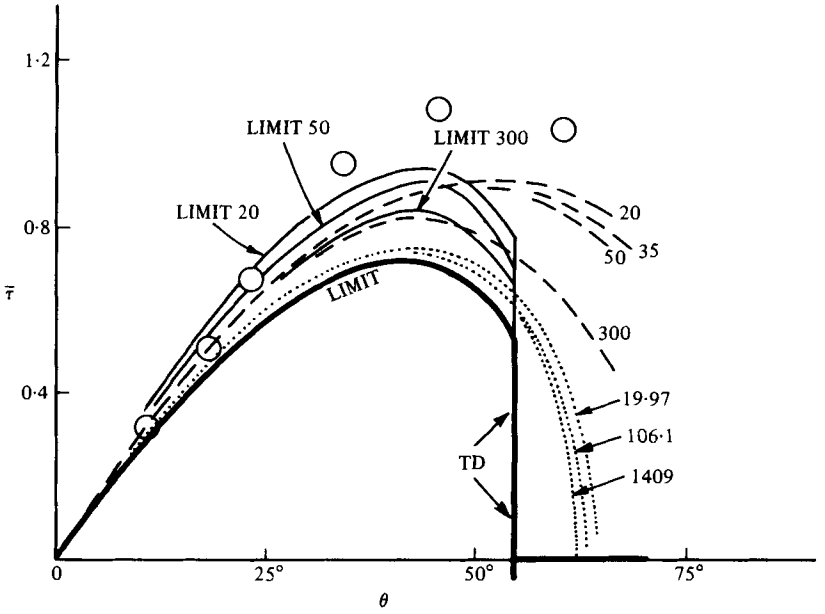

FIGURE 3. The skin friction $\bar{\tau} = (2\,Re)^{-\frac{1}{2}}\partial u/\partial n$ against θ, for the circular cylinder. The curve LIMIT is the boundary-layer solution from the Kirchhoff slip velocity, with TD denoting the (asymptotically abrupt) effect of the triple deck at $\theta = \theta_{sep} = 55°$. The dotted curves are $O(Re^{-\frac{1}{16}})$ modified boundary-layer solutions with Re values as shown. The curves LIMIT 20, LIMIT 50, LIMIT 300 include the effects (4.2), (4.3) of the back pressure (3.2*b*) when $Re = 20$, 50, 300 respectively. The dashed curves give the Navier–Stokes solutions of Dennis & Chang (1970, for $Re = 20$, 35, 50) and the (nearly steady) solution of Patel (1976, $Re = 300$). The circles are from the experiments of Dimopoulos & Hanratty (1968, $Re = 105$).

2.4. *Solving the main body-scale flow problems, and comparisons with experiments and Navier–Stokes solutions*

The particular bluff body considered here is the circular cylinder $x^2+y^2 = a^2$. First, the solution for the attached boundary layer III upstream of the separation point was calculated. The slip velocity induced by the leading-order free-streamline flow in I, with the smooth separation condition (2.1*a*), was deduced from Brodetsky's (1923) highly accurate approximation to the solution, and the finite-difference solution for the boundary layer was then marched forward from the front stagnation point ($\theta = 0$) to the onset of separation ($\theta = \theta_{sep} = 55°$, from Brodetsky 1923: see also Woods 1955). Two different grid sizes were used to check the accuracy, and the numerical solutions are believed to be accurate to at least three decimal places in the skin friction $\tau = \partial u(\theta, 0)/\partial N$. The solution is presented in figure 3. It gives the value

$$\lambda[\equiv \tau(\theta_{sep})] = 0{\cdot}72\,a^{\frac{1}{2}}.$$

Next, we obtained the modified inviscid flow field I, described by the first two terms of (2.2) together with the stipulation (2.3*a*) or (2.3*b*). Again the solution was based on Brodetsky's (1923) conformal-mapping approach. To include the singularity (2.3*b*), which implies infinite curvature of the free streamline, involves but a small change in Brodetsky's analysis. Thus his work remains unaltered until his equation (4) is

reached: then his (4) (which he applied to ensure smooth separation) is replaced by the condition

$$1+A_1-A_3+A_5-\ldots=-0{\cdot}44\,Re^{-\frac{1}{16}}\lambda^{\frac{9}{8}}, \tag{2.18}$$

which ensures (2.3a, b) at separation. Here and below we adopt Brodetsky's notation without alteration. To satisfy (2.13) we take [instead of his (7)]

$$A_1=-1+a_1+\epsilon, \quad A_3=a_1+a_3, \quad A_5=a_3+a_5, \ldots, \tag{2.19}$$

where ϵ is the right-hand side of (2.18). Note that his (7) contains a misprint: a_2 should read a_3. Now, to obtain a first approximation to the modified solution, we let all the constants a_i be zero except a_1. The constant a_1 is then determined by equating the radii of curvature of the body, both at its front stagnation point and at the separation point, to the (unknown) radius of the cylinder a (in the conformal-mapping method here a is not known in advance). This condition requires that

$$\frac{4\exp(-1+\frac{4}{3}a_1+\epsilon)}{1-\epsilon-2a_1}=\frac{2}{1-\epsilon+2a_1}=a. \tag{2.20}$$

Since

$$\epsilon=-0{\cdot}44\,Re^{-\frac{1}{16}}\lambda^{\frac{9}{8}}, \tag{2.21}$$

(2.20) yields two equations for the unknowns a_1 and a, given $\lambda=0{\cdot}72\,a^{\frac{1}{2}}$. In practice it proved more convenient to start a calculation by specifying the value of $a_1+\frac{4}{3}\epsilon$, then to solve (2.20) for $2a_1+\epsilon$ and a, which also yield the values of a_1 and ϵ, and finally to use (2.21) to deduce the corresponding Reynolds number Re. By varying the specified value of $a_1+\frac{4}{3}\epsilon$, we were then able to obtain the modified free-streamline solution for a wide range of Reynolds numbers. Once a_1, ϵ and a have been determined, the slip velocity outside the boundary layer III follows from Brodetsky (1923) [the equation immediately after his (5): he uses $r=1/q$], while

$$C_D=\pi(1+\tfrac{1}{2}A_1)^2, \tag{2.22}$$

$$\theta_{\text{sep}}=-A_1+\tfrac{1}{3}A_3-\tfrac{1}{5}A_5+\ldots. \tag{2.23}$$

We note in passing that the requirement (2.20) produces a body whose radius of curvature between $\theta=0$ and $\theta=\theta_{\text{sep}}$ deviates from that of the circular cylinder by about $3\frac{1}{2}\%$ at most (Brodetsky 1923) when $\epsilon=0$ ($Re\to\infty$). For the finite values of ϵ and Re that were used in the modified free-streamline solutions, this deviation was increased, but it never exceeded 5%. Also, an alternative, and more rigorous, treatment of the modified free-streamline flow may be adopted by taking $\epsilon\ll 1$ in (2.20) and (2.21). This yields the results (excluding terms of order ϵ^2)

$$\left.\begin{aligned} a_1&=0{\cdot}0574-0{\cdot}229\,\epsilon, \quad C_D=\pi(0{\cdot}5287)^2[1+1{\cdot}455\,\epsilon],\\ a&=1{\cdot}794+2{\cdot}342\,\epsilon, \quad \theta_{\text{sep}}=0{\cdot}9617-0{\cdot}820\,\epsilon. \end{aligned}\right\} \tag{2.24}$$

Finally, a second approximation to the modified solution may be found by taking both a_3 and a_1 to be non-zero in (2.19), which enables the radii of curvature of the body at $\theta=0$, at $\theta=\theta_{\text{sep}}$ and at an intermediate point to be set equal to a. Certainly, when $\epsilon=0$, this yields a more accurate approximation than before, the body's radius of curvature varying by at most a fraction of 1% between $\theta=0$ and $\theta=\theta_{\text{sep}}$

(see Brodetsky). The analysis for non-zero values of ϵ is similar to that of (2.20)–(2.24) and involves solving

$$\frac{4\exp(-1+\frac{4}{3}a_1+\epsilon+\frac{8}{15}a_3)}{1-\epsilon-2a_1-2a_3} = \frac{2}{1-\epsilon+2a_1-2a_3}$$
$$= \frac{2^{\frac{1}{2}}(2^{\frac{1}{2}}-1)\exp[2^{-\frac{1}{2}}(-1+\frac{2}{3}a_1+\epsilon-\frac{8}{15}a_3)]}{1-\epsilon+2a_3} = a, \quad (2.25)$$

where (2.21) still holds. In particular, for $\epsilon \ll 1$ we find

$$\left.\begin{aligned} a_1 = 0{\cdot}0585 - 0{\cdot}2996\,\epsilon, \quad a_3 = -0{\cdot}0083 - 0{\cdot}0871\,\epsilon, \\ a = 1{\cdot}760 + 2{\cdot}221\,\epsilon, \quad \theta_{\text{sep}} = 0{\cdot}9599 - 0{\cdot}8116\,\epsilon, \\ C_D = \pi(0{\cdot}52925)^2[1 + 1{\cdot}325\,\epsilon], \end{aligned}\right\} \quad (2.26)$$

excluding $O(\epsilon^2)$ effects.

The (modified) boundary layer III was then re-integrated forward from $\theta = 0$, with the modified slip velocity determined for a number of values of the Reynolds number. Strictly, in the limit as $\epsilon \to O$ ($Re \to \infty$), where the asymptotic theory is valid, the effect of the $O(Re^{-\frac{1}{16}})$ perturbation in the slip velocity is asymptotically small for

$$0 \leqslant \theta < \theta_{\text{sep}}$$

and the skin friction is almost unaltered from its previous form until the triple deck is reached. Moreover, a linearization akin to that of (2.24) or (2.26) is valid in III to deal with the small perturbation. However, in practice it is found that for moderate Reynolds numbers the $O(Re^{-\frac{1}{16}})$ disturbance is not unsubstantial, so it seems more sensible to re-solve the full boundary-layer equations for the modified

$$[O(1) + O(Re^{-\frac{1}{16}})]$$

flow field rather than solve the linearized equations for the $O(Re^{-\frac{1}{16}})$ disturbance: the two procedures are identical in the limit as $Re \to \infty$, in any case.

The numerical solutions for τ for the modified boundary layer† are presented in figure 3, together with the original unmodified solutions and results from experiments and Navier–Stokes solutions. The variables have been rescaled from those above in order to base the Reynolds number and the lengths on the cylinder radius. In figure 3, except near the front stagnation point, where the agreement is excellent, the unmodified solution for τ underestimates the experimentally observed and the numerical Navier–Stokes values (although, incidentally, the experimental results are themselves out of line with the Navier–Stokes solutions, possibly because of unsteadiness in practice). The inclusion of the $O(Re^{-\frac{1}{16}})$ effects, however, reduces this discrepancy, but generally only by a fairly small amount for the moderate values of Re at which reliable experimental and numerical results are available. The above discrepancies are not surprising when one views the pressure distribution on the cylinder (figure 4), for both the modified and the unmodified free-streamline solutions for the pressure

† Note that, for the $O(1)$ (rather than asymptotically small) values of ϵ used in the boundary-layer calculations, the skin friction τ always tends to zero *ahead of* the proposed separation position $\theta = \theta_{\text{sep}}$, because of the increasingly adverse pressure gradient as θ nears θ_{sep}. This feature is in line with the theory of § 2.1 and F. T. Smith (1977, p. 448), where $\epsilon \to 0$ and the true separation occurs within the triple deck. Also, the Goldstein (1948) singularity is approached at the onset of the false separation where $\tau \to 0+$.

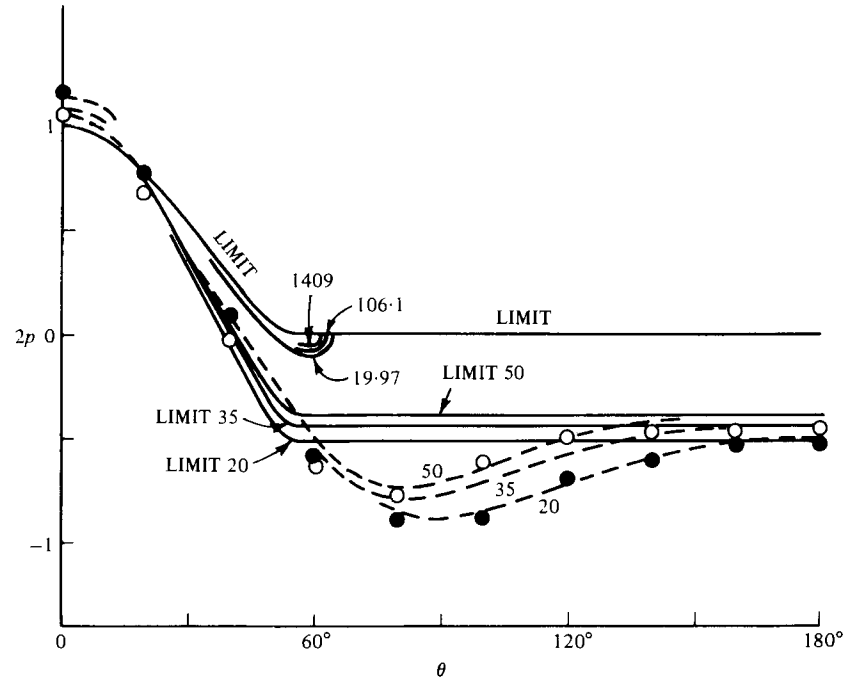

FIGURE 4. The pressure distribution on a circular cylinder. ----, Navier–Stokes solutions of Dennis & Chang (1970) for Re values shown; ●, ○, experimental values of Grove *et al.* (1964) for Re = 20, 88·5 respectively; LIMIT is the Kirchhoff solution; curves marked 19·97, 106·1, 1409 are the modified solutions at those Re values; curves LIMIT 50, LIMIT 35, LIMIT 20 give the effects [see (4.2), (4.3)] of the back pressure (3.2*b*) when Re = 50, 35, 20 respectively.

give less favourable pressure gradients overall (for $0 \leqslant \theta < \theta_{sep}$) than those of experiment and Navier–Stokes solutions. On the other hand, a more encouraging feature is the very close agreement as far as the initial variation of the pressure (and hence τ) near the front stagnation point is concerned. By contrast, further round the cylinder it is difficult to decide between the free-streamline pressure (and skin friction) distributions and those of the triple deck (F. T. Smith 1977) when comparisons are being made with experiments or Navier–Stokes solutions: for instance, a distance of unity on the triple-deck scale corresponds to an angle of 60° around the cylinder when Re = 50. This largeness of the separation regions partly explains the discrepancies in figures 3 and 4, we believe. Another, related, source of difficulty in comparisons is that even terms of the relatively small order $O(Re^{-\frac{1}{2}})$ can give a substantial contribution to certain quantities at moderate Reynolds numbers. This aspect is demonstrated in figures 3 and 4, which, in anticipation of the results (3.2*b*), (4.2) and (4.3) below, show the effects of the theoretical $O(Re^{-\frac{1}{2}})$ surface pressure π_E in the near-eddy II beyond separation. The inclusion of this $O(Re^{-\frac{1}{2}})$ effect in fact improves the agreement between the theory and experiments or calculations more than does the $O(Re^{-\frac{1}{16}})$ effect. Another demonstration of the practical importance of the $O(Re^{-\frac{1}{2}})$ terms rather than the $O(Re^{-\frac{1}{16}})$ terms will be given in § 5 below (see figure 11).

A final, and encouraging, comparison is made in figure 5 between the values of the pressure at the front stagnation point according to the present theory and from

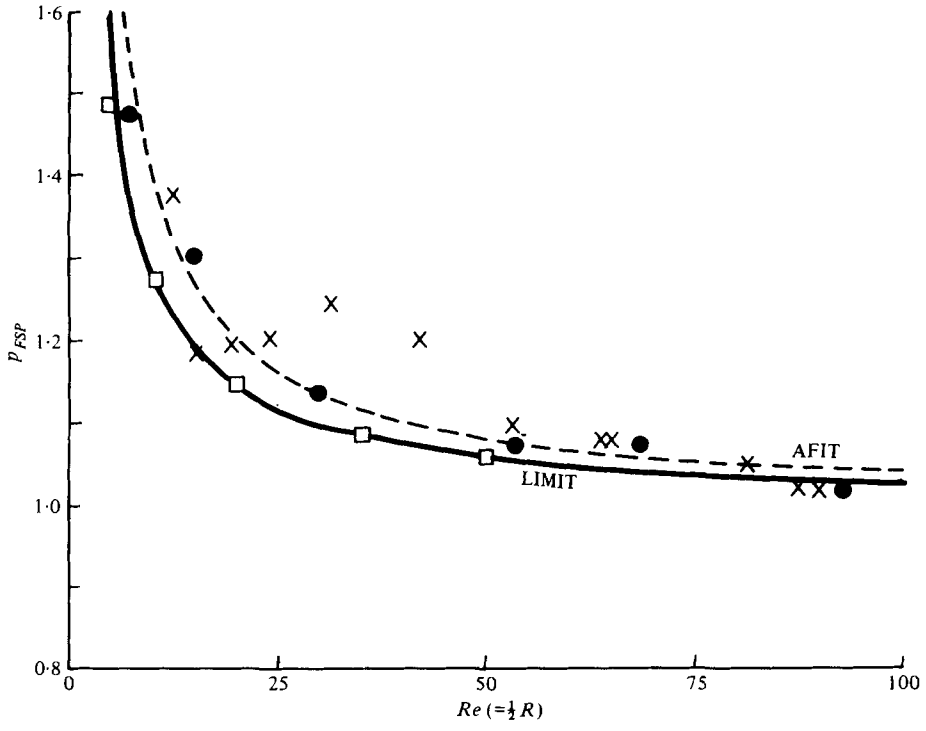

FIGURE 5. The front-stagnation-point pressure p_{FSP} ($= 2p$ at $n = \theta = 0$) as a function of Re. □, Navier–Stokes solutions of Dennis & Chang (1970); ×, ●, experimental values of Grove *et al.* (1964) and Homann (1936) respectively; LIMIT gives the prediction (2.27); AFIT gives (for comparison purposes) the prediction of attached flow inviscid theory.

experiments (Grove *et al.* 1964; Homann 1936) and Navier–Stokes solutions (Dennis & Chang 1970; Takami & Keller 1969). The present theory yields the asymptote

$$2p(0) = 1 + 5{\cdot}692/R, \tag{2.27}$$

where $R = 2Re$ is the Reynolds number based on the cylinder diameter. Dennis & Chang's (1970) Navier–Stokes calculations predict a numerical coefficient of 6·09 in (2.27), while Takami & Keller's (1969) predicted value is 5·985. By comparison, the attached inviscid flow model gives a coefficient of 8. Our result (2.27) is in excellent agreement with Dennis & Chang's calculations, even when $Re = 10$ (see figure 5), while the experimental variation also seems fairly in keeping with (2.27). Also, the agreement is slightly improved if we include the $O(Re^{-\frac{1}{16}})$ modification, which yields

$$2p(0) = 1 + (5{\cdot}692/R)\,(1 + 0{\cdot}0194\,R^{-\frac{1}{16}}). \tag{2.28}$$

Only (2.27) is shown in figure 5.

Considered *in toto*, the comparisons in figures 3–5 would seem to be not discouraging: the agreement at the front stagnation point (figure 5) or near it (in figures 3, 4) is excellent, while the discrepancies elsewhere (in figures 3, 4) are readily reconcilable with the multi-structured nature of the asymptotic flow model (see also §4). We turn now to a discussion of the broader-scale flow, to attempt to complete the flow picture for high Reynolds numbers.

3. The eddy properties, the reattachment and the wake beyond the eddy

3.1. *The eddy and reattachment*

The two major steps in attempting a broad description of the complete eddy of circulatory flow behind the body involve the determination of the eddy length and its shape (see also Sychev 1967; Messiter 1975). First, the length of the eddy must be $O(Re)$ to satisfy a condition of momentum conservation. This condition is the result

$$C_{D\infty} = 2\int(1-u)\,dy \tag{3.1}$$

stemming from integration of the Navier–Stokes momentum equations (see Batchelor 1967, p. 351). The integral in (3.1) extends across the half-wake $y \geqslant 0$ far downstream of the eddy and it defines the ultimate wake displacement, which must be finite since $C_{D\infty}$ is finite (from §2). Such a finite ultimate displacement can occur only if the wake displacement immediately behind the eddy is also finite. So, assuming that there is no great change in the velocity profile as the detached shear layer passes through reattachment to emerge at the start of the wake, we may conclude that the shear-layer displacement is also finite [i.e. that ψ is $O(1)$] within the shear layer just ahead of reattachment. But, from (2.13a), this demands that $x = O(Re)$ before reattachment. Hence the eddy length is $O(Re)$. (A precise determination of the length is given in §3.2 below.)

Second, the following argument may be advanced concerning the eddy shape. The property (2.9) suggests that the width of the eddy is $O(Re^{\frac{1}{2}})$, if a direct match is to be achieved between the complete eddy flow and the body-scale flow. Therefore the typical eddy slope is small and $O(Re^{-\frac{1}{2}})$. Outside the eddy the motion is then governed by the inviscid equations, on streamwise and transverse length scales $O(Re)$, and is a small $[O(Re^{-\frac{1}{2}})]$ perturbation of the uniform stream since the eddy acts effectively as a slender body. Hence pressures $O(Re^{-\frac{1}{2}})$ [in line with (2.11)] are provoked when x and y are $O(Re)$ and, for a general eddy shape, this leads to a non-uniform pressure distribution $O(Re^{-\frac{1}{2}})$ just outside the eddy. The pressure changes by less than $O(Re^{-\frac{1}{2}})$ across the shear layer [which bounds the eddy and reduces the velocity from $O(1)$ outside the eddy to $o(1)$ inside], so, from the balance of momentum, the velocity u is $O(Re^{-\frac{1}{4}})$ within the eddy. Then conservation of mass demands that $\psi = O(Re^{\frac{1}{4}})$ in the eddy. But in the shear layer ψ is only $O(1)$ [see previous paragraph and (2.14d)], as it is also in the body flow (§2) and near the line of symmetry $y = 0$. Consequently, there is no mechanism for entrainment of this $O(Re^{\frac{1}{4}})$ mass flux. So, to a large extent, the flow in the eddy has a closed streamline pattern and rotates clockwise between the shear layer and the line of symmetry.

Given that the length and thickness of the eddy are $O(Re)$ and $O(Re^{\frac{1}{2}})$ respectively, the only real chance of a breakdown in the above argument lies in the assumption that the $O(Re^{-\frac{1}{2}})$ pressure at the shear layer is non-uniform. For if, and only if, the (slender) eddy shape is *elliptical* then the $O(Re^{-\frac{1}{2}})$ eddy pressure is uniform. In fact, from linearized potential flow theory the pressure, on the $O(Re)$ length scale, is given by

$$p = Re^{-\frac{1}{2}}\mathscr{R}\left[-\hat{a} - \frac{\hat{a}}{2}\frac{L-2Z}{Z^{\frac{1}{2}}(-L+Z)^{\frac{1}{2}}}\right] \tag{3.2a}$$

to leading order [$\mathscr{R}$ denotes the real part, and $Z = X + iY$, where $(x, y) = Re(X, Y)$]. Here the eddy ellipse has the form $Y = \hat{a}X^{\frac{1}{2}}(L-X)^{\frac{1}{2}}$, so that LRe is the unknown eddy length (see § 3.2), and $\hat{a} = bL^{-\frac{1}{2}}$ to match with the initial form (2.9). Moreover, from (3.2*a*) the uniform pressure in the eddy, and hence in the near-eddy II of § 2, is

$$-\hat{a}Re^{-\frac{1}{2}},$$

i.e.

$$p(=\pi_E) = -(4C_{D\infty}/\pi L)^{\frac{1}{2}}Re^{-\frac{1}{2}} + o(Re^{-\frac{1}{2}}) \quad \text{in} \quad \text{II} \tag{3.2b}$$

from (2.10). Again, we note that (3.2*a*) matches the large-length-scale pressure with that of the body-scale flow, (2.11), as required.

The second possibility (*b*) above, that of an elliptical shape, is the one we favour in this paper and is an attractive one, of course. For the elliptical shape preserves the spirit of the body flow structure of § 2, in that the velocity within the eddy is small and is only $O(Re^{-\frac{1}{2}})$ if the eddy flow is driven entirely by the entrainment into the shear layer [in which case a match with the near-eddy behaviour of (2.14*d*) is obtained]. Moreover, the eddy's shape is then completely (and quite simply) determined once its length LRe has been found (see § 3.2 below), since the starting form (2.9) may be used to fix the elliptical eddy's width. In particular, from (2.9), the maximum half-width H of the eddy is given by

$$H = (C_{D\infty}L/\pi)^{\frac{1}{2}}Re^{\frac{1}{2}} + o(Re^{\frac{1}{2}}) \tag{3.2c}$$

if possibility (*b*) holds. The possibility (*b*) is analogous to the uniform-pressure eddy model successfully adopted by Burggraf (1975) and Jenson *et al.* (1974). In contrast, the first possibility (*a*), that of an $O(Re^{-\frac{1}{2}})$ pressure variation in the eddy, almost certainly involves a numerical treatment of the nonlinear eddy flow. The possibility (*a*) would tend to move the eye (or node) of the eddy more towards the eddy centre however, whereas in the case of possibility (*b*) the eye could (but does not necessarily have to†) lie asymptotically close [on the $O(Re)$ length scale] to the reattachment point. But, apart from that feature, the existence of the recirculating eddy implied by possibility (*a*) appears to serve no real purpose, since the eddy velocities are too small to affect the fluid entrainment by the shear layer. Comparisons between the possibility (*b*) and experimental or calculated eddy flows will be presented in § 3.3 below.

In either case, on the eddy length scale $x = ReX$, where X is finite, the flow field divides into four basic zones (see figure 6). Zone (i) is the outer inviscid zone of linearized potential flow; (ii) is the viscous shear layer of thickness $O(1)$, from (2.13*a*); (iii) is the eddy of width $O(Re^{\frac{1}{2}})$ between zone (ii) and the line BC, where B contains the body flow and C the reattachment; and zone (iv) is the viscous wake of thickness $O(1)$ (see § 3.2) downstream of C. Zone (ii) is controlled by the viscous-shear-layer problem (2.12*a–c*) again, and we may assume its solution to be given by (2.13*a*) throughout $0 < X < L$, i.e.

$$\psi = X^{\frac{1}{2}}G(\hat{\eta})\,[\hat{\eta} \equiv \hat{n}/X^{\frac{1}{2}}] \quad \text{in} \quad \text{(ii)}. \tag{3.3}$$

But the main properties of zones (i) and (iii) depend on which, if either, of the possibilities (*a*) and (*b*) introduced above is correct. It is impossible to decide conclusively between those two (and other) possibilities without a detailed knowledge of the flow properties near the reattachment point of the shear layer (at C in figure 6). At C the

† For instance, a pressure variation greater than $O(Re^{-1})$ but less than $O(Re^{-\frac{1}{2}})$, consistent with possibility (*b*), would keep the eye towards the eddy centre, as in (*a*).

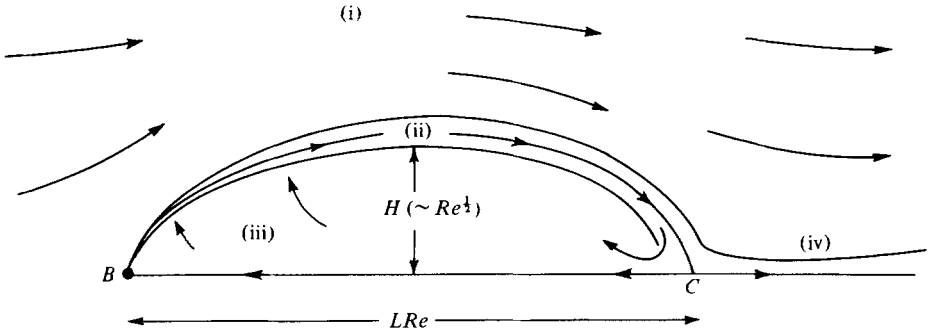

FIGURE 6. The large-scale structure, comprising the linearized potential flow (i), viscous shear layer (ii), eddy (iii) and ultimate viscous wake (iv). The point B contains the body-scale flow and C is the reattachment point.

shear layer (ii) splits into two, the fluid below the dividing streamline $\psi = 0$ being reversed in order to supply the eddy flow (iii), while the remainder of the shear layer ($\psi \geqslant 0$) continues into the wake (iv). The point at which this reversal takes place ($X = L$) is determined by momentum conservation (see §3.2). The actual means for this reversal are not yet clear, however: to date, the only consistent description found for a large-scale reattachment similar to ours appears to be that of Messiter *et al.* (1973), and their approach applied in the present context implies that a backward jet emanates from C, the velocity and thickness of the jet both being $O(1)$. The existence of such a backward jet is inconsistent with our overall flow model, but an alternative description of reattachment to that of Messiter *et al.* (1973) is not forthcoming yet.

While a complete account of the reattachment and eddy flows would be most desirable, instead we are led to postulate here that an alternative description of reattachment exists† which is consistent with our overall flow model [including the possibility (*b*)] above. Given postulate (*b*), and assuming that the reattachment process preserves the vorticity of the incoming shear-layer profile through C, we can now move on to determine one of the major remaining unknowns, the eddy length L.

3.2. *The wake beyond reattachment, and the determination of the eddy length*

Immediately downstream of the reattachment at C, a velocity profile $u = U_W(y)$, $\psi = \Psi_W(y)$ emerges, with $y = O(1)$ and the properties $U_W(\infty) = 1$, $\Psi_W(0) = 0$ and $U_W(0) > 0$. This profile forms the starting profile for the (finite thickness) viscous wake [(iv) in figure 6] downstream of the eddy.

In (iv), ψ, u and y are $O(1)$, $x = ReX$ with X finite and $X > L$, but $p = O(Re^{-\frac{1}{2}})$ from §3.1. Hence the wake is controlled by the boundary-layer equations

$$u = \frac{\partial \psi}{\partial y}, \quad u\frac{\partial u}{\partial X} - \frac{\partial \psi}{\partial X}\frac{\partial u}{\partial y} = \frac{\partial^2 u}{\partial y^2} \tag{3.4a}$$

with initial conditions

$$u = U_W(y), \quad \psi = \Psi_W(y) \quad \text{at} \quad X = L^+ \tag{3.4b}$$

† Another point of view, similar to one adopted by Messiter *et al.* (1973), is to regard the flow structure (i)–(iv) as a reasonable first approximation, with the influence of a backward jet to be incorporated later to improve the approximation. Such a view seems optimistic in our problem, however.

and boundary conditions

$$\psi = 0 = \partial u/\partial y \quad \text{at} \quad y = 0, \tag{3.4c}$$

$$u \to 1 \quad \text{as} \quad y \to \infty. \tag{3.4d}$$

The solution of (3.4*a–d*) depends on the initial profile in (3.4*b*), which has to be fixed from the reattachment properties considered in § 3.1. Far downstream, however, as $X \to \infty$, the following asymptotic form is to be expected:

$$\left.\begin{aligned} \psi &\approx X^{\frac{1}{2}}\hat{\eta} - g(\hat{\eta}) + o(1), \\ u &\approx 1 - X^{-\frac{1}{2}} g'(\hat{\eta}) + o(X^{-\frac{1}{2}}), \end{aligned}\right\} \tag{3.5}$$

where $\hat{\eta} = y/X^{\frac{1}{2}}$ and $g'(\hat{\eta}) = \beta\pi^{-\frac{1}{2}} \exp(-\frac{1}{4}\hat{\eta}^2)$, from (3.4*a, c, d*). The constant $\beta = g(\infty)$ (effectively, the ultimate wake displacement) is dependent upon the full solution to (3.4*a–d*). In fact, since

$$\beta = \int_0^\infty (1-u)\,dy \quad \text{for} \quad X \gg 1,$$

from (3.1) we have

$$C_{D\infty} = 2\beta, \tag{3.6}$$

so that, since $C_{D\infty}$ is given (from the body flow in region I in § 2), (3.6) determines β, which in turn determines the value of L through the effect of L on the initial profile (3.4*b*).

From the assumption made at the end of § 3.1, that vorticity is conserved through the reattachment, we may now propose (cf. Messiter *et al.* 1973; Burggraf 1970, 1975; Jenson *et al.* 1974) that the initial profile in (3.4*b*) is described by the shear layer form (ii) at $X = L^-$, since the latter form does preserve the vorticity. Thus we have

$$\Psi_W(y) = L^{\frac{1}{2}} G(y/L^{\frac{1}{2}}) \quad (\text{for } y > 0) \tag{3.7}$$

from (3.3). The controlling influence of L on Ψ_W is clearly exhibited by (3.7). Now, however, L can be factorized out of the wake calculation by setting

$$(\psi, u, X, y) = (L^{\frac{1}{2}}\overline{\psi}, \overline{u}, L\overline{X}, L^{\frac{1}{2}}\overline{y}), \tag{3.8}$$

for then $\overline{\psi}(\overline{X}, \overline{y})$ and $\overline{u}(\overline{X}, \overline{y})$ satisfy (3.4*a*) and (3.4*c, d*) again, with X and y replaced by $\overline{X}$ and $\overline{y}$, but the initial conditions

$$\overline{\psi} = G(\overline{y}), \quad \overline{u} = G'(\overline{y}) \quad \text{at} \quad \overline{X} = 1 \tag{3.9}$$

[with $G(0) = 0$ now imposed] hold in place of (3.4*b*). Integration of (3.4*a, c, d*) for $\overline{X} > 1$ can therefore proceed without prior knowledge of L. Let us denote the factorized displacement $\lim_{\overline{y} \to \infty} [\overline{y} - \overline{\psi}(\overline{X}, \infty)]$ by $\overline{\beta}(\overline{X})$. Then (3.9) and (3.6) imply that

$$\beta = L^{\frac{1}{2}}\overline{\beta}(\infty)$$

and

$$C_{D\infty} = 2L^{\frac{1}{2}}\overline{\beta}(\infty). \tag{3.10}$$

A central-difference numerical solution was obtained for the factorized problem of the wake, (3.4*a, c, d*) with (3.9). A complication arises at the start of the integration ($\overline{X} \to 1+$), where there exists a double structure (cf. Goldstein 1930). First, for

$$0 < \overline{X} - 1 \ll 1$$

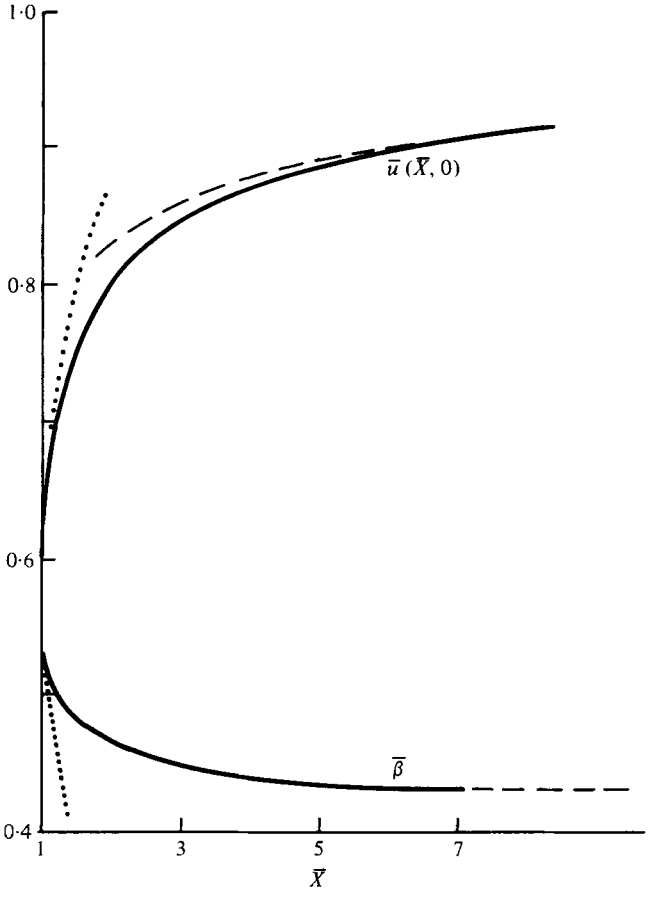

FIGURE 7. The numerical solutions for the factorized displacement thickness $\bar{\beta}$ and centre-line velocity $\bar{u}(\bar{X}, 0)$ of the ultimate wake (iv) [see (3.4*a*, *c*, *d*), (3.9)]. The dots give the starting behaviour (3.15) and the dashes give the large-$\bar{X}$ asymptote [see (3.5)] based on the value

$$\bar{\beta}(\infty) = 0{\cdot}43.$$

the solution when $\bar{y}$ is $O(\bar{X}-1)^{\frac{1}{2}}$ ($\bar{y} = (\bar{X}-1)^{\frac{1}{2}}\bar{\eta}$, say) may be expanded in the form

$$\left.\begin{aligned} \bar{\psi} &= (\bar{X}-1)^{\frac{1}{2}}c_0\bar{\eta} + (\bar{X}-1)\,\bar{G}_1(\bar{\eta}) + O(\bar{X}-1)^{\frac{3}{2}}, \\ \bar{u} &= c_0 + (\bar{X}-1)^{\frac{1}{2}}\bar{G}_1'(\bar{\eta}) + O(\bar{X}-1), \end{aligned}\right\} \tag{3.11}$$

where, from (3.4*a*), (3.9) and (3.4*c*),

$$\bar{G}_1(\bar{\eta}) = \tfrac{1}{2}c_1\bar{\eta}^2 - \frac{2c_1}{(\pi c_0)^{\frac{1}{2}}}\int_0^{\bar{\eta}} \eta_1 \left\{\int_\infty^{\eta_1} \frac{\exp(-\frac{1}{4}c_0\eta_2^2)}{\eta_2^2}\,d\eta_2\right\} d\eta_1. \tag{3.12}$$

Here we have used the feature $G(\bar{y}) \approx c_0\bar{y} + \frac{1}{2}c_1\bar{y}^2 + \ldots$ for $\bar{y} \ll 1$, where $c_0 = 0{\cdot}587$ and $c_1 \doteqdot 0{\cdot}21$ are given constants, from (2.13). Also, we know that $G \sim \bar{y} - \bar{\beta}_0$ for $\bar{y} \gg 1$, where $\bar{\beta}_0 = 0{\cdot}533$ [$\equiv \bar{\beta}(0)$]. Second, when $\bar{y}$ is $O(1)$ and $0 < \bar{X} - 1 \ll 1$,

$$\left.\begin{aligned} \bar{\psi} &= G(\bar{y}) + (\bar{X}-1)\,G_1(\bar{y}) + \ldots, \\ \bar{u} &= G'(\bar{y}) + (\bar{X}-1)G_1'(\bar{y}) + \ldots, \end{aligned}\right\} \tag{3.13}$$

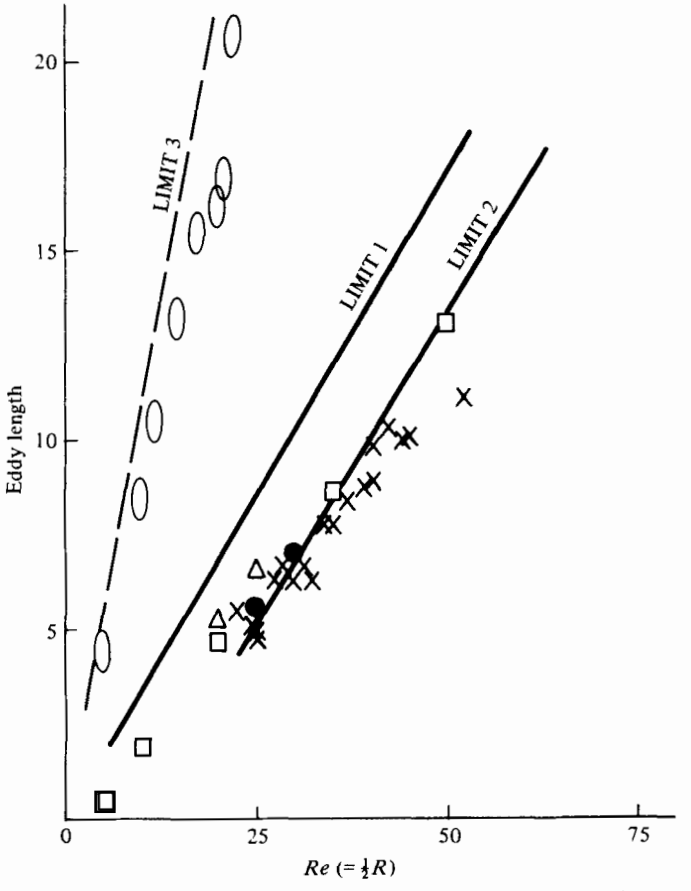

FIGURE 8. The eddy length as a function of Reynolds number. For the circular cylinder: □, ●, △, calculated results of Dennis & Chang (1970), Takami & Keller (1969), Kawaguti & Jain (1966) respectively; ×, experimental results of Acrivos *et al.* (1968); LIMIT 1 gives the prediction (3.16) and LIMIT 2 is (3.16) with an origin shift in *Re*. For the normal flat plate: ○, from Batchelor (1967) and Acrivos *et al.* (1968); LIMIT 3 gives (3.16).

where $G_1(0) = c_1/c_0$ to match (3.13) with (3.11). Substitution into (3.4*a*) yields

$$G_1(\bar{y}) = G'(\bar{y}) \left\{ \frac{G_1(0)}{c_0} + \int_0^{\bar{y}} \frac{G'''(y_1)\, dy_1}{G'(y_1)^2} \right\}. \tag{3.14}$$

The solutions in (3.14) and (3.12) give the properties

$$\left.\begin{aligned} \bar{\beta}(\bar{X}) &\approx \bar{\beta}_0 + (\bar{X}-1)[\tfrac{1}{2}\bar{\beta}_0 - c_1/c_0^2] + o(\bar{X}-1) \\ \bar{u}(\bar{X},0) &\approx c_0 + 2c_1(\pi c_0)^{-\frac{1}{2}}(\bar{X}-1)^{\frac{1}{2}} + o(\bar{X}-1)^{\frac{1}{2}} \end{aligned}\right\} \quad \text{for} \quad 0 < \bar{X}-1 \ll 1 \tag{3.15}$$

for the wake displacement and centre-line velocity initially. To accommodate this singular structure in the numerical scheme we adopted Smith's (1974) procedure of using a two-region numerical approach, at the start of the integration in $\bar{X} > 1$, marching in uniform steps of $(\bar{X}-1)^{\frac{1}{2}}$. The solutions are presented in figure 7 and agree well with (3.15) initially. The similarity form (3.5) is approached ultimately

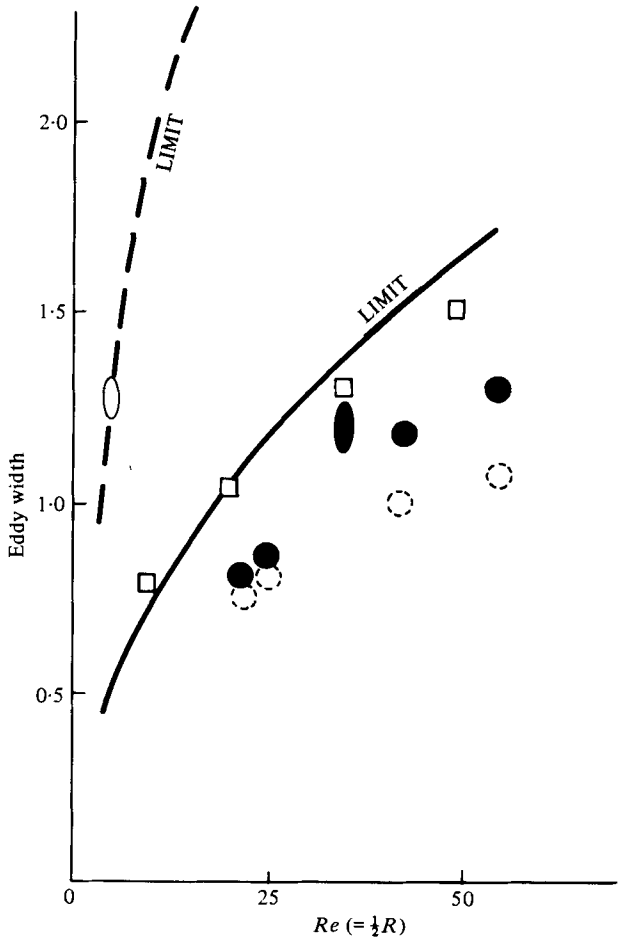

FIGURE 9. The eddy width as a function of Reynolds number. For the circular cylinder: □, Dennis & Chang's (1970) Navier–Stokes solutions; ●, experimental values of Grove *et al.* (1964) corrected for wind-tunnel interference (see appendix); ○, uncorrected experimental values; ——, prediction (3.2*c*). For the normal flat plate: ○, from Batchelor (1967) and Acrivos *et al.* (1968); – – –, from (3.2*c*).

downstream (figure 7) and the calculations gave the value $\bar{\beta}(\infty) = 0{\cdot}43$. From (3.10), therefore, the formula

$$L = 1{\cdot}36\, C_{D\infty}^2 \tag{3.16}$$

determines the eddy length ($= LRe$).

3.3. *Comparisons of eddy length, width and pressure with experiments and Navier–Stokes solutions*

In figures 8 and 9 the prediction (3.16) for the eddy length and the result (3.2*c*) for the maximum eddy width are compared with experimental or calculated values, for the circular cylinder and the broadside-on flat plate in particular. The Reynolds number Re here is based on the cylinder radius or plate half-width.

First, figure 8 plots the eddy length as a function of Reynolds number Re for the circular cylinder. The prediction (3.16) (which yields $L = 0{\cdot}34$ since $C_{D\infty} = 0{\cdot}50$) shows

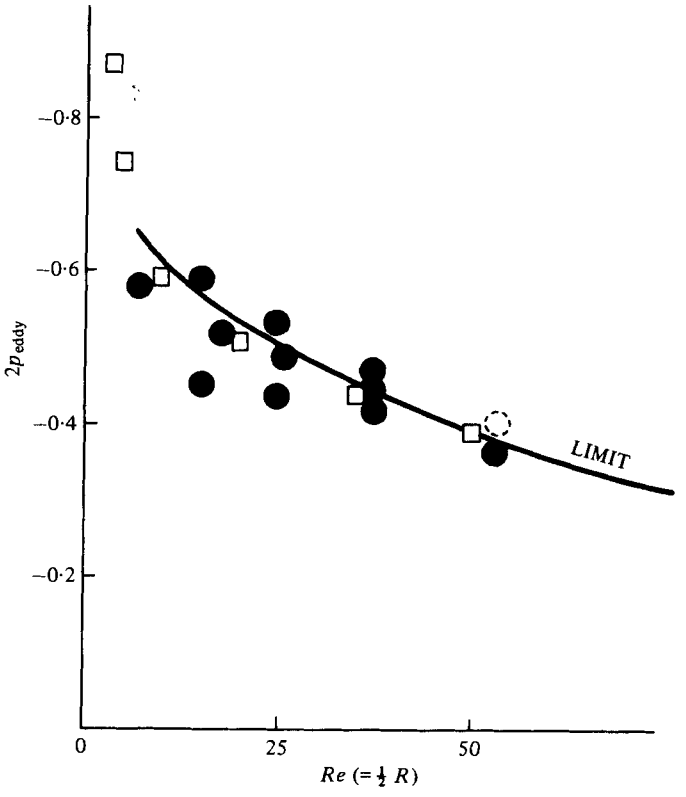

FIGURE 10. Variation of the eddy pressure with Reynolds number, for the circular cylinder. □, calculations of Dennis & Chang (1970); ●, ○, experiments (Grove *et al.* 1964; Acrivos *et al.* 1968), with and without wind-tunnel correction respectively (see appendix); LIMIT, the prediction (3.2*b*).

very good agreement with the experimental and calculated Navier–Stokes variations; indeed, if the origin for the Reynolds number is slightly shifted then (3.16) fairly accurately follows the practical and calculated values down to Reynolds numbers as low as 20. Second, figure 8 also presents eddy-length results for the broadside-on flat plate (for which $C_{D\infty} = 0{\cdot}88$). Few experimental or calculated results for laminar flow seem to be availablefor comparison; those shown in figure 8 have been read from plate 4 of Batchelor (1967) and from the experiments of Acrivos *et al.* (1968). The agreement with (3.16) (which yields $L = 1{\cdot}055$, since $C_{D\infty} = 0{\cdot}88$) is again good, even though the value of Re is as low as 5 in the experiments. We note in passing that the large-scale theory of §§ 3.1 and 3.2 does include the cases of non-smooth bluff bodies like this flat plate, since the theory relies only on the initial existence of a shear layer dividing the free stream from the virtually stagnant eddy beneath. Thus (3.16) is a universal formula for any bluff-body flow.

Third, figure 9 concerns the maximum width of the eddy. The experimental results therein have been read from the figures of Grove *et al.* (1964), Batchelor (1967, plate 4) and Acrivos *et al.* (1968), while the Navier–Stokes results have been read from the figures of Dennis & Chang (1970). For the circular cylinder the prediction (3.2*c*) (which yields $H = 0{\cdot}233\ Re^{\frac{1}{2}}$) for $Re \gg 1$ is not inconsistent with the calculated widths, particularly if allowance is made for an origin shift in the value of Re. The experimental

values of the eddy width are themselves at variance with the Navier–Stokes solutions, owing possibly to unsteadiness or to wind-tunnel interference. Professor D. W. Moore kindly suggested that an investigation of tunnel-wall effects would be desirable and an analysis (given in the appendix) indicates that the tunnel walls used in the experiments did exert a significant influence on the observed values of eddy width, as figure 9 shows. In the results for the broadside-on flat plate also shown in figure 9 the comparison with (3.2c) (which yields $H = 0{\cdot}544\ Re^{\frac{1}{2}}$) is again fairly good.

Lastly, in figure 10, experimental and calculated values of the pressure at the rear stagnation point of the circular cylinder are plotted against the Reynolds number, along with the prediction (3.2b) [which gives $p = -1{\cdot}37\ Re^{-\frac{1}{2}} + o(Re^{-\frac{1}{2}})$ from (3.16)]. The agreement is very encouraging indeed. As we shall see in §§4 and 5, the rear stagnation point and near-eddy pressure of (3·2b), while an order of magnitude smaller than the pressure [$O(1)$] acting on the body upstream of separation, nevertheless still provides a most significant contribution to the drag on the body at moderate Reynolds numbers. Also, the work in the appendix indicates that, again, the experimental values of eddy pressure are significantly affected by the presence of tunnel walls. One example of the wall effect is presented in figure 10; other examples are presented in the appendix (figure 12–14).

4. The effect of the $O(Re^{-\frac{1}{2}})$ eddy pressure on the body-scale flow

Returning to consider the body-scale flow, we wish now to include the influence of the $O(Re^{-\frac{1}{2}})$ eddy pressure (which is clearly of importance in practice: see figure 4). From (3.2a) the pressure behaviour required in the outer reaches of the body-scale flow is

$$p \sim \tfrac{1}{2}i\hat{a}(L/z)^{\frac{1}{2}} + \ldots - \hat{a}\,Re^{-\frac{1}{2}} + o(Re^{-\frac{1}{2}}) \tag{4.1}$$

for $|z| \gg 1$, where $z = x + iy$. Here the leading term matches with (2.11), but the $O(Re^{-\frac{1}{2}})$ term gives the predominant effect of the large-scale flow of § 3 on the body-scale flow of § 2. We notice that this 'back-pressure' term is present uniformly at large distances in the body-scale flow; it does *not* act solely in the eddy (cf. Roshko 1954, 1955; Riabouchinsky 1919; Gilbarg & Serrin 1950; and others).

The modifying effect of the back pressure may be incorporated rationally and quite simply into the original body-scale flow of § 2 as a small perturbation. For its presence means that the body-scale flow is subjected to an effective free-stream pressure (i.e. for $|z| \to \infty$, but $|Z| \ll 1$) of π_E rather than the true free-stream pressure (holding for $|Z| \gg 1$) of zero. Similarly the free-stream velocity for the body-scale flow is effectively $1 - \pi_E$ rather than 1, because of the small velocity increase produced by the existence of the large-scale eddy. Hence an effective rescaling of the flow variables of § 2 is produced, in the sense that the values of p and q determined in § 2 are to be re-interpreted as the values of $(p - \pi_E)/(1 - \pi_E)^2$ and $q/(1 - \pi_E)$, from the non-dimensionalization introduced in § 1. [We stress that, here and elsewhere, we are excluding the small effects due to boundary-layer and shear-layer displacement or to the adjustments near separation.] So, if the flow variables of § 2 are now given the subscripts K, the actual pressure and speed p and q are given by

$$p = \pi_E + (1 - \pi_E)^2 p_K, \quad q = (1 - \pi_E)\, q_K. \tag{4.2}$$

Again, the skin friction τ (and hence the value of λ) determined in § 2 must be multiplied by $(1-\pi_E)^{\frac{3}{2}}$ to incorporate the back-pressure effect, and Re also suffers a re-scaling. Thus

$$\tau = (1-\pi_E)^{\frac{3}{2}}\tau_K, \quad Re = (1-\pi_E)\,Re_K. \tag{4.3}$$

It is a simple matter, therefore, to re-interpret all the solutions of § 2 in order to take account of the main influence of the large-scale flow of § 3.

The rational rescalings of (4.2) and (4.3) have dramatic effects on the body-scale flow solutions at moderate Reynolds numbers, as figures 3 and 4 demonstrate for the circular cylinder. Thus in figure 4, for $Re = 50$, say, the theoretical pressure (4.2) follows very closely the distribution of the Navier–Stokes solutions up to the onset of separation; through separation the triple-deck solutions of F. T. Smith (1977) then yield fairly close agreement with the calculated forms [the value $2\lambda = 1{\cdot}8$ used by Smith (1977) was extracted from the Navier–Stokes solutions and should be replaced by $2\lambda = 1{\cdot}44\,(1-\pi_E)^{\frac{3}{2}}$, but this replacement alters his comparisons only marginally]; finally the eddy pressure (3.2*b*) agrees well with that of the Navier–Stokes solutions near the rear of the cylinder. Again, the skin-friction prediction undergoes a substantial alteration (figure 3) because of the back-pressure effect (4.3) and the theory now falls very much in line with the Navier–Stokes solutions.

We re-emphasize that many previous studies (Riabouchinsky 1919; Gilbarg & Serrin 1950; Roshko 1954, 1955; Parkinson & Jandali 1970; Kiya & Arie 1977; Birkhoff & Zarantonello 1957) have been based (wrongly, we believe) on the belief that the back pressure acts only within the eddy, whereas our approach shows that the back pressure also acts on the free-stream conditions as far as the body-scale flow is concerned.

5. Further comparisons and discussion

Two criticisms which in the past have often been levelled at the (extended) Kirchhoff model of the body flow may now be answered. The first criticism is that the model underestimates the observed values of the near-eddy pressure. The answer is provided in figure 10, which shows that the lower-order terms in the asymptotic expansion (of which the Kirchhoff solution forms the leading term in the body-scale flow) produce contributions which, even at moderate Reynolds numbers, agree very well with the observed values. In fact, the present theory leads to a new, rational, interpretation of the role played by the back pressure; for, in contrast with previous studies, this work shows that not only is the back pressure asymptotically small but also, on the body scale, it acts *within the free stream as well as within the eddy*. The true free-stream conditions are attained only on the much larger length scale of the eddy flow.

The second major criticism of the Kirchhoff model is that it badly underpredicts the observed drag. Again, the answer is provided by the lower-order terms in the asymptotic expansion, as follows. For the circular cylinder ($x^2+y^2 = 1$), to calculate the theoretical pressure drag C_{DP}, first we include both the major body-scale flow terms $C_{D\infty} + O(Re^{-\frac{1}{16}})$ determined in § 2.4 and the near-eddy pressure contribution from (3.2*b*) (which gives the surface pressure between the rear stagnation point $\theta = 180°$ and the separation point $\theta = \theta_{\text{sep}} = 55°$). The result is presented in figure 11(*a*) and compared with Dennis & Chang's (1970) calculated values. The agreement is very encouraging. For, although at $Re = 50$, say, the Kirchhoff model *per se* predicts only

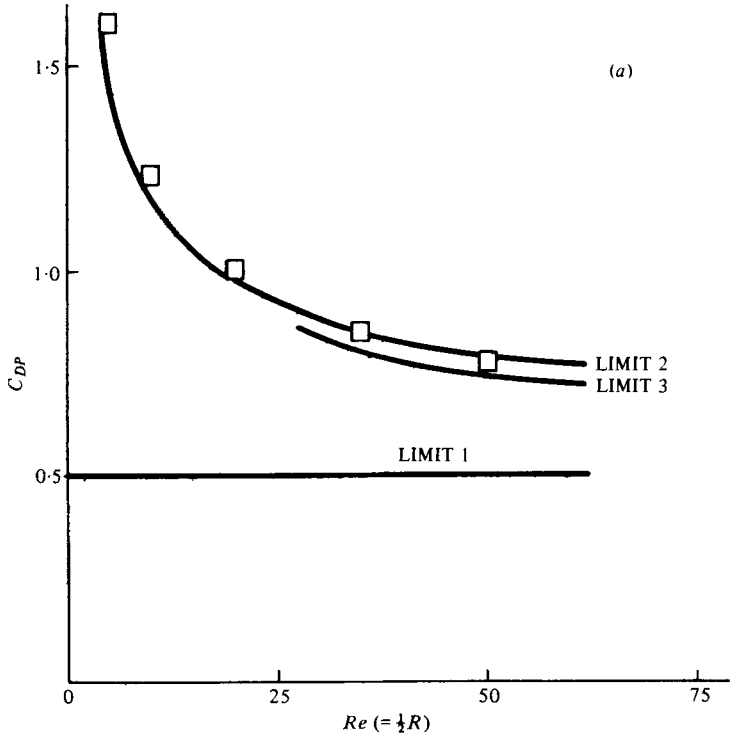

Figure 11 (*a*). For legend see facing page.

about 65 % of the calculated pressure drag, the $O(Re^{-\frac{1}{2}})$ contribution from the near-eddy pressure raises the prediction to within 4 % of the calculated value! An alternative approach suggested by § 4 is to include the back pressure as a rescaling effect (as in figures 3 and 4), implying that the Kirchhoff pressure drag $C_{D\infty}$ is multiplied by $(1-\pi_E)^2$. Again the agreement so obtained (figure 11*a*) is remarkably good. The total drag C_D, obtained by adding to C_{DP} the friction drag C_f from the modified boundary-layer solutions of § 2.4, is given in figure 11 (*b*), along with calculated and experimental values. In the curve LIMIT 2 in figure 11 (*b*), the back pressure π_E is included only within the eddy (as in the curve LIMIT 2 in figure 11*a*). Here again the inclusion of the $O(Re^{-\frac{1}{2}})$ effects, i.e. both C_f and the near-eddy pressure (3.2*b*), serves greatly to improve the drag prediction, from 47·4 % [for the $O(1)$ terms alone] to about 85 % [for the terms $O(1)+O(Re^{-\frac{1}{16}})+O(Re^{-\frac{1}{2}})$] of the observed or calculated values at $Re = 50$. In the curve LIMIT 3 in figure 11 (*b*) the rescaling effects of (4.2) and (4.3) are adopted, both in C_f and in $C_{D\infty}$ (as in the curve LIMIT 3 of figure 11*a*). The differences between the theory and experiments or Navier–Stokes solutions are again about 15 % at $Re = 50$.

Some other important features of the bluff-body flow have been equally, or even more, supportive of the extended Kirchhoff model. Examples are the comparisons of eddy length and front-stagnation-point pressure in figures 5 and 8. Also, although by contrast some discrepancies do appear to show up initially in other aspects such as the skin-friction and pressure plots in figures 3 and 4 (except near the front stagnation point), these discrepancies also can be ascribed to lower-order effects (see, for example, the back-pressure effects in figures 3 and 4). It is hoped that the same explanation will

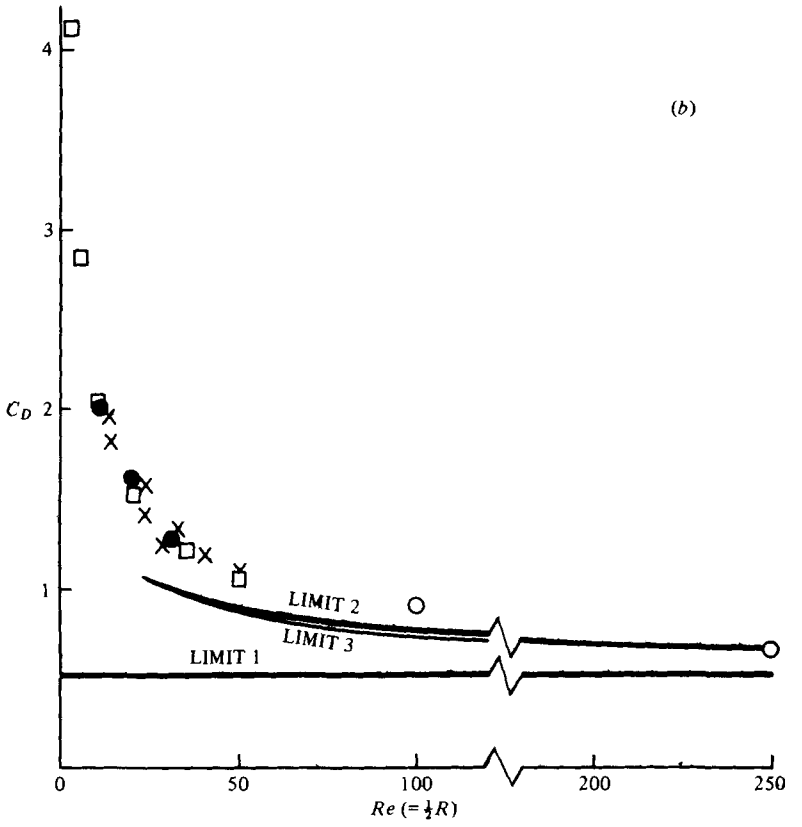

FIGURE 11. (*a*) The dependence of the pressure drag C_{DP} on Re, for the circular cylinder. LIMIT 1 is the Kirchhoff value (Brodetsky 1923), LIMIT 2 includes the extra effect of both the $O(Re^{-\frac{1}{16}})$ terms and the eddy pressure (3.2*b*), LIMIT 3 includes the rescaling effects (4.2) and (4.3), and the open squares are the numerical results of Dennis & Chang (1970). (*b*) The dependence of the total drag C_D on Re, for the circular cylinder. □, ●, the steady Navier–Stokes solutions of Dennis & Chang (1970), Takami & Keller (1969) respectively; ○, the (nearly steady) numerical solutions of Son & Hanratty (1969), ×, experimental results of Tritton (1959). LIMIT 1 is the Kirchhoff value (Brodetsky 1923); LIMIT 2 includes the extra effect of $O(Re^{-\frac{1}{16}})$ terms and of the eddy pressure and friction drag; LIMIT 3 includes the $O(Re^{-\frac{1}{2}})$ effects (4.2), (4.3) of the back pressure (3.2*b*).

apply to the position of the separation point, where the predictions in (2.24) or (2.26) are in poor agreement with the observed or calculated values; it is noteworthy in this context that the free-streamline model does give excellent predictions of the separation point, as well as the drag, in internal flows (see Smith 1979; Deshpande, Giddens & Mabon 1976).

We may now deal with a third criticism made of the present theoretical model. This criticism is that, if the relative error in the theory is of order $Re^{-\frac{1}{16}}$, then the theory cannot be relevant at the moderate Reynolds numbers for which steady laminar flow is possible. The comparisons in figures 3–4 and 8–11 and the formulae (2.24), (2.26) and (2.28) are enough to silence this third criticism, we suggest. For, although $Re^{-\frac{1}{16}}$ is not a small number there, the coefficients of the $Re^{-\frac{1}{16}}$ terms are so small as to make the $O(Re^{-\frac{1}{16}})$ contributions almost negligible (even when $Re = 10$, say). Indeed, the $O(Re^{-\frac{1}{16}})$ contribution is much less important practically than the $O(Re^{-\frac{1}{2}})$ contri-

butions, as figures 4, 10 and 11 show. Thus the asymptotic theory does appear to be relevant at moderate Reynolds numbers, giving good predictions for the most important flow properties: the drag, eddy length, eddy width, the eddy pressure and the front-stagnation-point pressure. The sole remaining doubt in the theory concerns the motion near reattachment (§ 3.1). Like Jenson *et al.* (1974) and Burggraf (1975), we propose a passive behaviour there, with the flow reversal dominated by the necessary entrainment into the shear layer.

Finally, the work in the appendix leads to the conclusion that the presence of confining walls in wind-tunnel experiments produces a substantial distortion of the eddy properties even when the walls are far apart. Thus, for example, the present theoretical prediction (§ 3), of an unlimited growth ($\propto Re^{\frac{1}{2}}$) of the eddy width as Re increases, and the experimental observations (Grove *et al.* 1964; Acrivos *et al.* 1965, 1968), of an upper bound on the eddy width, *are* reconcilable [see figure 9 above and figure 12 and equation (A 13) below] since the observed behaviour is largely a direct consequence of the presence of the confining walls. Similarly, the experimental observation of a non-zero limit for the eddy pressure, as Re increases, is a direct result of the flow confinement [as figure 10 above and figures 12–14 and equation (A 14) below suggest] rather than a feature of the unbounded flow problem. Hence any theory based solely on the above experimental results, and not compensating for the wind-tunnel effects, is bound to be inappropriate for the unbounded flow problem, we believe. In particular, almost all the fundamentals of the theory of Acrivos *et al.* (1965, 1968) can be explained in terms of the distorting influence of confining walls on the present model [figures 12–14 and equations (A 13) and (A 14) below]. We conclude, therefore, that the Acrivos *et al.* (1965, 1968) theory is not appropriate to the unbounded flow problem.

After the completion of the present work the author received copies of Sychev's (1967) and Messiter's (1975) papers, kindly supplied by Professor A. F. Messiter and Mr J. H. B. Smith respectively. Both papers contain material and viewpoints having much in common with §§ 3.1 and 3.2. In particular, as Professor Messiter (private communication) pointed out, Sychev (1967) also proposed the elliptical eddy and determined its length. Sychev's eddy-length calculation [based on the momentum deficit integral of (3.4a), without calculating the whole wake solution] is more direct than that of § 3.2 and yields the result $\bar{\beta}(\infty) = 2c_1 \doteq 0{\cdot}42$. The ensuing alterations in the formulae for L, H and π_E are fairly slight, however, and disturb the comparisons in figures 8–11 only minimally. Messiter (1975) also made a number of other intriguing speculations. More recently, Messiter (1978) has reviewed many aspects of separation and eddies, and J. H. B. Smith (1977) and F. T. Smith (1978) have examined the separation of a three-dimensional vortex sheet from a smooth surface, again coming essentially to the viewpoint of Sychev (1972) and Smith (1977) of incompressible separation.

I am very grateful to Professor A. F. Messiter and Mr J. H. B. Smith for their constructive comments on this paper, and also to Professor A. Acrivos, Professor S. C. R. Dennis, Professor A. F. Messiter, Professor D. W. Moore, Professor N. Riley, Mr J. H. B. Smith and Professor K. Stewartson for informative and stimulating discussions on various aspects of the bluff-body problem. In particular, Professor D. W. Moore is thanked for emphasizing the desirability of an investigation of wind-tunnel effects (see appendix).

Appendix. On the effects of confining walls

An examination of the possible effects of confining, wind-tunnel, walls on the theoretical flow pattern seems called for. We consider a wide tunnel, aligned with the uniform stream and of width $2h$ Re much greater than the body dimensions but still comparable with the dimensions of the large-scale flow of § 3.

To leading order the influence of such confining walls is to restrict the domain of the linearized potential flow in zone (i) outside the eddy (figure 6). The flow problem in (i) may be stated in terms of the disturbance stream function ψ_1, where

$$\psi = Y\,Re + Re^{-\frac{1}{2}}\psi_1 + o(Re^{\frac{1}{2}})$$

in (i). Thus ψ_1 satisfies $\nabla^2\psi_1 = 0$ together with the boundary conditions

$$\psi_1 = 0 \quad \text{at} \quad Y = h \quad (-\infty < X < \infty), \tag{A 1}$$

$$\psi_1 = 0 \quad \text{at} \quad Y = 0 \quad \text{for} \quad X < 0 \quad \text{or} \quad X > L, \tag{A 2}$$

$$\partial\psi_1/\partial y = \hat{a} \quad \text{at} \quad Y = 0 \quad \text{for} \quad 0 < X < L, \tag{A 3}$$

$$\psi_1 \to 0 \quad \text{as} \quad |X| \to \infty, \tag{A 4}$$

where $-\hat{a}\,Re^{-\frac{1}{2}}\,(= \pi_E)$ is the unknown constant eddy pressure. Also, to match with the body-scale flow (2.9)–(2.11) we require

$$\psi_1 \sim -b(X^2+Y^2)^{\frac{1}{4}}\cos(\tfrac{1}{2}\phi) \quad \text{as} \quad (X, Y) \to (0, 0). \tag{A 5}$$

It is convenient to work in terms of the modified complex potential

$$\overline{w}(\bar{Z}) = \phi_1 + i\psi_1 - \hat{a}\bar{Z},$$

where ϕ_1 is the disturbance velocity potential and $\bar{Z} = (X+iY) - \frac{1}{2}(L+ih)$. By symmetry the domain of interest may then be confined to the semi-infinite strip $\mathscr{R}(\bar{Z}) \leqslant 0$, $|\mathscr{I}(\bar{Z})| \leqslant \frac{1}{2}h$ (here $\mathscr{I}$ denotes the imaginary part), with the symmetry condition $\partial\psi_1/\partial X = 0$ along $\mathscr{R}(\bar{Z}) = 0$. We let A, B, O, D and E denote the points $\bar{Z} = -\infty - \frac{1}{2}hi$, $-\frac{1}{2}L - \frac{1}{2}hi$, $0 - \frac{1}{2}hi$, $0 + \frac{1}{2}hi$ and $-\infty + \frac{1}{2}hi$ respectively and map the interior of the strip $ABODE$ to the upper half of the ζ plane by the conformal map

$$\zeta = \sin(\pi\bar{Z}/ih). \tag{A 6}$$

The points A, B, O, D and E map to the points A', B', O', D' and E' on the real ζ axis, where $(A', B', O', D', E') = (-\infty, -\kappa, -1, 1, \infty)$ and $\kappa = \cosh(\pi L/2h)$.

The $\overline{w}$ plane may also be mapped to a half-plane. For if $\overline{w} = \overline{\phi} + i\overline{\psi}$ then the flow field is the semi-infinite strip $\overline{\phi} \geqslant c$, $-\hat{a}h \leqslant \overline{\psi} \leqslant 0$, where c is an arbitrary potential constant. The points in the $\overline{w}$ plane corresponding to A, B, O, D and E are, respectively, $A'' = \infty + 0i$, $B'' = c + 0i$, $O'' = c - \mu\hat{a}hi$, $D'' = c - \hat{a}hi$ and $E'' = \infty - \hat{a}hi$, where $0 < \mu < 1$ and $-\mu\hat{a}h$ is the unknown value of $\overline{\psi}$ at O. The mapping

$$\zeta = -\sin\left[\frac{\pi}{ih\hat{a}}\,(\overline{w} - c + \tfrac{1}{2}\hat{a}hi)\right] \tag{A 7}$$

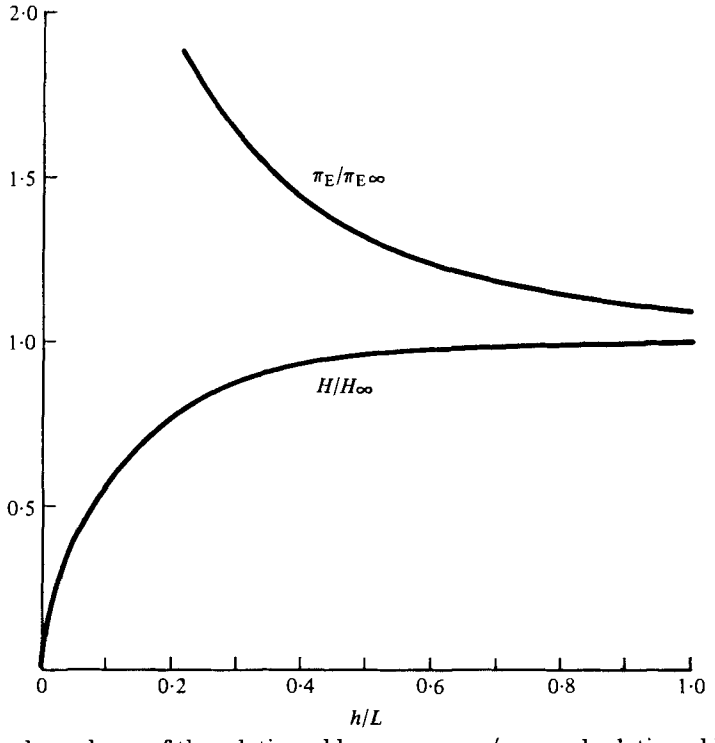

FIGURE 12. The dependence of the relative eddy pressure π_E/π_{E_∞} and relative eddy width H/H_∞ on the ratio (tunnel half-width)/(eddy length) = h/L, according to (A 9), (A 11).

then takes the flow field to the upper half of the $\tilde{\xi}$ plane, the points A'', B'', O'', D'' and E'' mapping to the points $\tilde{\xi} = -\infty$, -1, β, 1 and ∞ on the real $\tilde{\xi}$ axis, or A''', B''', O''', D''' and E''', respectively. Here $\beta = -\cos(\mu\pi)$.

Finally, the ζ and $\tilde{\xi}$ planes are related by the mapping $\zeta = \tilde{a}\tilde{\xi} + \tilde{b}$, where, to identify the points A', B', O', D' and E' and A''', B''', O''', D''' and E''' respectively, the constants $\tilde{a}$ and $\tilde{b}$ satisfy $\tilde{a}+\tilde{b} = 1$, $\tilde{a}\beta+\tilde{b} = -1$ and $-\tilde{a}+\tilde{b} = -\kappa$. In terms of $\overline{w}$ and $\overline{Z}$, therefore, we have the flow solution

$$\frac{1-\kappa}{2} - \frac{1+\kappa}{2}\cos\left[\frac{\pi}{i\hat{h}\hat{a}}(\overline{w}-c)\right] = \sin\frac{\pi\overline{Z}}{i\hat{h}}, \tag{A 8}$$

where the constant $\hat{a}$ is determined from the condition (A 5), giving

$$\hat{a} = -\frac{1}{2}\left(\frac{\pi}{\hat{h}}\right)^{\frac{1}{2}}\left(\frac{\kappa+1}{\kappa-1}\right)^{\frac{1}{4}} b\,[= \pi_E Re^{\frac{1}{8}}]. \tag{A 9}$$

The eddy shape, $Y = Re^{-\frac{1}{8}}S_E(X)$, say, follows from (A 8) by working out the value of $-\psi_1$ along BO. Hence

$$S_E(X) = -\frac{h\hat{a}}{\pi}\cos^{-1}\left[\frac{2}{1+\kappa}\left(\frac{1-\kappa}{2} + \cosh\left(\frac{\pi X}{h}\right)\right)\right]. \tag{A 10}$$

Also the maximum width of the eddy occurs at $X = \frac{1}{2}L$ and is

$$H = \frac{1}{2}\left(\frac{h}{\pi}\right)^{\frac{1}{2}}\left(\frac{\kappa+1}{\kappa-1}\right)^{\frac{1}{4}} b\,Re^{\frac{1}{8}}\cos^{-1}\frac{3-\kappa}{1+\kappa}. \tag{A 11}$$

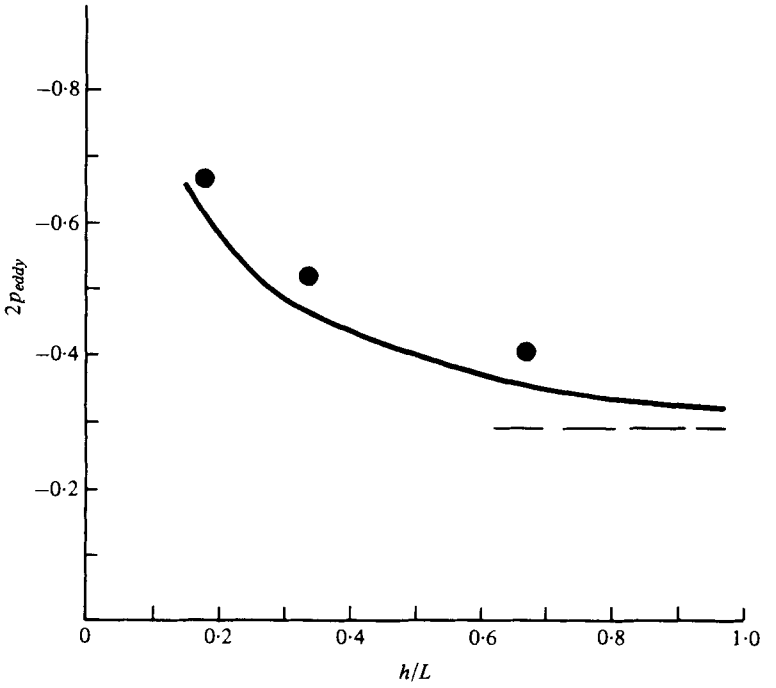

FIGURE 13. Comparisons between theoretical [——, from (A 9)] and experimental (●, from Grove *et al.* 1964) eddy pressures when $Re = 87{\cdot}5$, for various ratios h/L [= 0·0336 (tunnel width)/(cylinder diameter)]. The dashed line gives the theoretical result for unbounded flow, (3.2*b*).

For a given tunnel half-width h and Reynolds number Re the confined flow is therefore determined. Solution curves for H and π_E as functions of h/L are drawn in figure 12. A check on (A 9)–(A 11) confirms that as $h/L \to \infty$ ($\kappa \to 1$) the ideal, unbounded, situation of § 3.1 is retrieved, with $H/H_\infty \sim 1 - \frac{1}{90}(\pi L/4h)^4$ and

$$\pi_E/\pi_{E\infty} \sim 1 + \tfrac{1}{24}(\pi L/2h)^2, \quad \text{where} \quad H_\infty \quad \text{and} \quad \pi_{E\infty}$$

denote the values of H and π_E in the unbounded flow (of §§ 3 and 4). We turn now to comparisons with circular-cylinder experiments conducted in wind tunnels by Grove *et al.* (1964; see also Acrivos *et al.* 1965, 1968). Their eddy shapes (see their figures 10–13) were obtained for a value of the ratio (tunnel width)/(cylinder diameter) of 5. As we have shown, the primary important parameter is instead the ratio of the tunnel half-width to the eddy length, i.e. h/L. The first comparison is given in figure 13, where for a fixed value of Re the pressure at the rear stagnation point, i.e. π_E in (A 9), is found to be broadly in agreement with the experimental values for various (tunnel width)/(cylinder diameter) ratios. In particular, it is found that the presence of the confining walls is responsible for about 75 % of the difference between experiment and unbounded flow theory when the (tunnel width)/(cylinder diameter) ratio is 10 and for 60–70 % when this ratio is 20. The second comparison made concerns the eddy pressure π_E for a fixed (tunnel width)/(cylinder diameter) ratio and various Reynolds numbers, and is shown in figure 14. The agreement with the experimental results is again fairly satisfactory. The third comparison has already been made, in figure 9, where the influence of the confining walls [in (A 11)] is shown to induce a substantial

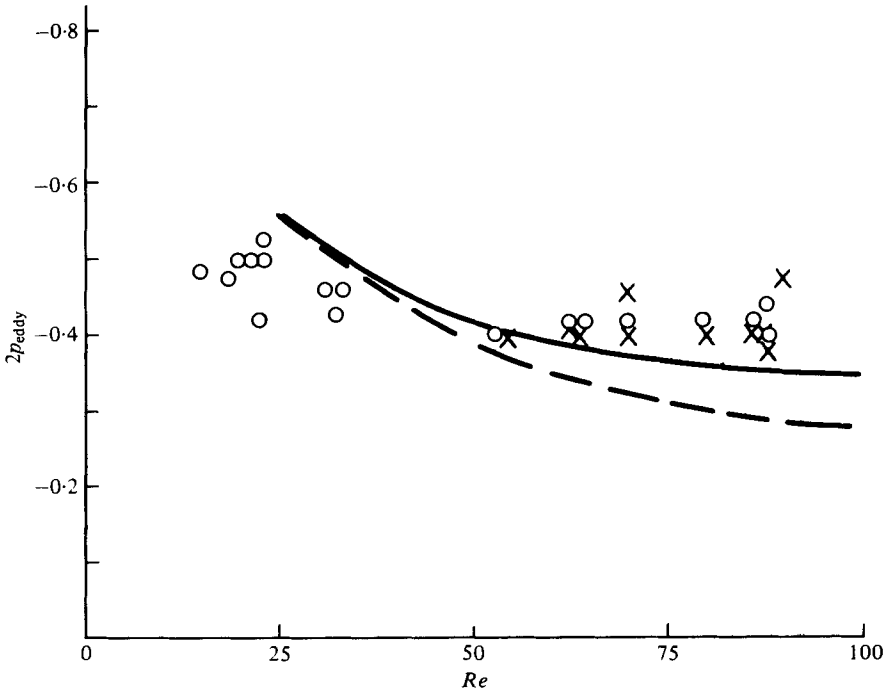

FIGURE 14. The eddy pressure as a function of Re for a given wind tunnel [with (tunnel width)/(cylinder diameter) = 20]. ○, experiments (Grove *et al.* 1964); ×, experiments (Acrivos *et al.* 1965); ——, present theory [equation (A 9)]; – – –, unbounded flow theory [(3.2*b*), included for comparison purposes].

effect on the maximum eddy widths, bringing the experiments much more into line with the (unbounded flow) theory and hence with the Navier–Stokes solutions of Dennis & Chang. The effects of the confining walls account largely for the observed tendency (Grove *et al.* 1964; Acrivos *et al.* 1965, 1968) for the eddy width to level out as Re increases. Indeed, for a fixed tunnel half-width $h\,Re = \hat{h}$, say, the levelling-out is bound to occur as Re increases, according to (A 10) and (A 11), since the governing parameter is $h/L = \hat{h}/L\,Re$, where $L = 0{\cdot}34$ for the circular cylinder. So, as Re increases, $h/L \to 0$ and from (A 10) the eddy shape formally acquires the form

$$y = \left(\frac{\hat{h}}{\pi}\right)^{\frac{1}{2}} \frac{b}{2} \cos^{-1}(-1 + 2e^{-\pi X/h}) \tag{A 12}$$

for $1 \ll \hat{h} \ll LRe$, and $0 < X < L$, while the maximum eddy width becomes

$$H = \tfrac{1}{2}b(\pi\hat{h})^{\frac{1}{2}} \quad \text{for} \quad 1 \ll \hat{h} \ll LRe. \tag{A 13}$$

Both the results (A 12) and (A 13) are independent of the Reynolds number. So, for a given wind tunnel and cylinder, the ultimate trend as Re increases is a levelling-out of the H *vs.* Re graph, in keeping with the experiments, whereas in the unbounded situation the growth $H \propto Re^{\frac{1}{2}}$ is appropriate, as the comparisons with the Navier–Stokes solutions in figure 9 verify. A similar levelling-out can be seen in the variation of the eddy pressure π_E as we let Re increase but keep the tunnel half-width $\hat{h}$ fixed. For, from (A 9),

$$\pi_E = -\tfrac{1}{2}(\pi/\hat{h})^{\frac{1}{2}}b \quad \text{for} \quad 1 \ll \hat{h} \ll LRe, \tag{A 14}$$

so again the ultimate trend is towards a plateau value (figure 14) in contrast with the decay $\pi_E \propto Re^{-\frac{1}{2}}$ appropriate to the unbounded situation (see figure 10). We may conclude therefore that the theory of Acrivos *et al.* (1965, 1968), which is founded on the wind-tunnel experiments of Grove *et al.* and Acrivos *et al.* (1965, 1968) and assumes $O(1)$ values for π_E and H, is not appropriate to the unbounded flow problem. Its features are almost all due to the presence of the confining tunnel walls [as in (A 13) and (A 14)].

Finally, one notes that the body-scale flow also is probably rather strongly affected by the confining walls (see Grove *et al.* 1964, figures 10–12, plate 2), that the body shape probably influences the confined flow of (A 1)–(A 11) in practice (Grove *et al.*, figures 10–12), and that the boundary-layer displacement at the tunnel walls would also tend to suppress the growth of the eddy width.

REFERENCES

ACRIVOS, A., LEAL, L. G., SNOWDEN, D. D. & PAN, F. 1968 Further experiments on steady separated flow past bluff objects. *J. Fluid Mech.* **34**, 25.

ACRIVOS, A., SNOWDEN, D. D., GROVE, A. S. & PETERSEN, E. E. 1965 The steady separated flow past a circular cylinder at large Reynolds numbers. *J. Fluid Mech.* **21**, 737.

BATCHELOR, G. K. 1956 A proposal concerning laminar wakes behind bluff bodies at large Reynolds numbers. *J. Fluid Mech.* **1**, 388.

BATCHELOR, G. K. 1967 *An Introduction to Fluid Dynamics.* Cambridge University Press.

BIRKHOFF, G. & ZARANTONELLO, E. H. 1957 Jets, wakes and cavities. *Appl. Math. Mech.* **2**.

BRODETSKY, S. 1923 Discontinuous fluid motion past circular and elliptic cylinders. *Proc. Roy. Soc.* A **102**, 542.

BURGGRAF, O. R. 1970 *U.S. Air Force Aerospace Res. Lab. Rep.* ARL 70-0275.

BURGGRAF, O. R. 1975 Asymptotic theory of separation and reattachment of a laminar boundary layer on a compression ramp. *AGARD Paper* no. 168 (on flow separation).

DENNIS, S. C. R. & CHANG, G.-Z. 1970 Numerical solutions for steady flow past a circular cylinder at Reynolds numbers up to 100. *J. Fluid Mech.* **42**, 471.

DESHPANDE, M. D., GIDDENS, D. P. & MABON, R. F. 1976 Steady laminar flow through modelled vascular stenoses. *J. Biomech.* **9**, 165.

DIMOPOULOS, H. G. & HANRATTY, T. J. 1968 Velocity gradients at the wall for flow around a cylinder for Reynolds numbers between 60 and 360. *J. Fluid Mech.* **33**, 303.

FÖPPL, L. 1913 Wirbelbewegung hinter einem Kreiszylinder. *Munich Akad. Wiss., Math.-Phys. Classe* no. 1.

GILBARG, D. & SERRIN, J. 1950 Free boundaries and jets in the theory of cavitation. *J. Math. Phys.* **29**, 1.

GOLDSTEIN, S. 1930 Concerning some solutions of the boundary layer equations in hydrodynamics. *Proc. Camb. Phil. Soc.* **26**, 1.

GOLDSTEIN, S. 1948 On laminar boundary layer flow near a point of separation. *Quart. J. Mech. Appl. Math.* **1**, 43.

GROVE, A. S., SHAIR, F. H., PETERSEN, E. E. & ACRIVOS, A. 1964 An experimental investigation of the steady separated flow past a circular cylinder. *J. Fluid Mech.* **19**, 60.

HOMANN, F. 1936 Einfluss grösser Zähigkeit bei Strömung um Zylinder. *Forsch. Ing. Wes.* **7**, 1.

IMAI, I. 1953 Discontinuous potential flow as the limiting form of the viscous flow for vanishing viscosity. *J. Phys. Soc. Japan* **8**, 399.

JENSON, R., BURGGRAF, O. R. & RIZZETTA, D. P. 1974 Asymptotic solution for supersonic viscous flow past a compression corner. *Proc. 4th Int. Conf. Numer. Meth. in Fluid Mech.* p. 218. Springer.

KAWAGUTI, M. 1953 Discontinuous flow past a circular cylinder. *J. Phys. Soc. Japan.* **8**, 403.

KAWAGUTI, M. & JAIN, P. C. 1966 Numerical study of a viscous flow past a circular cylinder. *J. Phys. Soc. Japan* **21**, 2055.

KIRCHHOFF, G. 1869 Zur Theorie freir Flüssigkeitsstrahlen. *J. reine angew. Math.* **70**, 289.

KIYA, M. & ARIE, M. 1977 An inviscid bluff-body wake model which includes the far-wake displacement effect. *J. Fluid Mech.* **81**, 593.

LOCK, R. C. 1951 The velocity distribution in the laminar boundary layer between parallel streams. *Quart. J. Mech.* **4**, 42.

LIGHTHILL, M. J. 1949 A note on cusped cavities. *Aero. Res. Counc. R. & M.* no. 2328.

MESSITER, A. F. 1975 Laminar separation – a local asymptotic flow description for constant pressure downstream. *AGARD Paper* no. 168 (on flow separation).

MESSITER, A. F. 1978 Boundary-layer separation. *U.S. Appl. Mech. Cong.*, University of California, Los Angeles.

MESSITER, A. F. & ENLOW, R. L. 1973 A model for laminar boundary layer flow near a separation point. *SIAM J.* **25**, 655.

MESSITER, A. F., HOUGH, G. R. & FEO, A. 1973 Base pressure in laminar supersonic flow. *J. Fluid Mech.* **60**, 605.

PARKINSON, G. V. & JANDALI, T. 1970 A wake source model for bluff body potential flow. *J. Fluid Mech.* **40**, 577.

PATEL, V. A. 1976 Time-dependent solutions of the viscous incompressible flow past a circular cylinder by the method of series truncation. *Computers & Fluids* **4**, 13.

RIABOUCHINSKY, D. 1919 On the steady flow motions with free surfaces. *Proc. Lond. Math. Soc.* **19**, 206.

ROSHKO, A. 1954 A new hodograph for free streamline theory. *N.A.C.A. Tech. Note* no. 3168.

ROSHKO, A. 1955 On the wake and drag of bluff bodies. *J. Aero. Sci.* **22**, 124.

ROSHKO, A. 1967 A review of concepts in separated flow. *Proc. Can. Cong. Appl. Mech., Quebec*, vol. 3, p. 81.

SHAIR, F. H. 1963 Ph.D. thesis, University of California, Berkeley.

SMITH, F. T. 1974 Boundary layer flow near a discontinuity in wall conditions. *J. Inst. Math. Appl.* **13**, 127.

SMITH, F. T. 1977 The laminar separation of an incompressible fluid streaming past a smooth surface. *Proc. Roy. Soc.* A **356**, 443.

SMITH, F. T. 1978 Three-dimensional viscous and inviscid separation of a vortex sheet from a smooth non-slender body surface. *R.A.E. Tech. Rep.* TR 78095.

SMITH, F. T. 1979 The separating flow through a severely constricted symmetric tube. *J. Fluid Mech.* **90**, 725.

SMITH, F. T. & DUCK, P. W. 1977 Separation of jets or thermal boundary layers from a wall. *Quart. J. Mech. Appl. Math.* **30**, 143.

SMITH, J. H. B. 1977 Behaviour of a vortex sheet separating from a smooth surface. *R.A.E. Tech. Rep.* TR 77058.

SON, J. S. & HANRATTY, T. J. 1969 Numerical solution for the flow around a cylinder at Reynolds numbers of 40, 200 and 500. *J. Fluid Mech.* **35**, 369.

SOUTHWELL, R. V. & VAISEY, G. 1946 Fluid motions characterized by free streamlines. *Phil. Trans. Roy. Soc.* A **240**, 117.

SQUIRE, H. B. 1934 On the laminar flow of a viscous fluid with vanishing viscosity. *Phil. Mag.* **17**, 1150.

STEWARTSON, K. 1974 Multistructured boundary layers on flat plates and related bodies. *Adv. Appl. Mech.* **14**, 145.

SYCHEV, V. YA. 1967 On laminar fluid flow behind a blunt body at high Reynolds numbers. *Rep. to 8th Symp. Recent Problems in Mech. Liquids & Gases, Tarda, Poland.*

SYCHEV, V. YA. 1972 Concerning laminar separation. *Izv. Akad. Nauk SSSR, Mekh. Zh. Gaza* **3**, 47.

TAKAMI, H. & KELLER, H. B. 1969 Steady two-dimensional viscous flow of an incompressible fluid past a circular cylinder. *Phys. Fluids Suppl.* **12**, II 51.

TRITTON, D. J. 1959 Experiments on the flow past a circular cylinder at low Reynolds numbers. *J. Fluid Mech.* **6**, 547.

Woods, L. C. 1955 Two dimensional flow of a compressible fluid past given curved obstacles with infinite wakes. *Proc. Roy. Soc.* A **227**, 367.

Wu, T. Y. 1956 A free streamline theory for two-dimensional fully cavitated hydrofoils. *J. Math. Phys.* **35**, 236.

Wu, T. Y. 1962 A wake model for free streamline flow theory. *J. Fluid Mech.* **13**, 161.

Wu, T. Y. 1968 Inviscid cavity and wake flows. *Basic Develop. in Fluid Dyn.* **2**, 1.

Wu, T. Y. 1972 Cavity and wake flows. *Ann. Rev. Fluid Mech.* **4**, 243.